

# Exploring structural requirements for peripherally acting 1,5-diaryl pyrazole-containing cannabinoid 1 receptor antagonists for the treatment of obesity

Mayank Kumar Sharma<sup>1</sup> · Prashant R. Murumkar<sup>1</sup> · Rajani Giridhar<sup>1</sup> · Mange Ram Yadav<sup>1</sup>

Received: 15 October 2014 / Accepted: 1 July 2015 / Published online: 17 July 2015  
© Springer International Publishing Switzerland 2015

**Abstract** Peripherally acting cannabinoid 1 (CB1) receptor antagonists are considered as potential therapeutics for the treatment of obesity with desired efficacy and reduced central nervous system side effects. A dataset of 72 compounds containing the 1,5-diaryl pyrazole basic skeleton having peripheral CB1 receptor antagonistic activity was utilized for three-dimensional quantitative structure–activity relationship studies. Compounds of the series exhibited high variations in the biological activity and chemical structures. Different types of molecular alignments, such as atom-based, data-based, centroid-based and centroid/atom-based were utilized to develop the best CoMFA model. The best CoMFA model was obtained with a database alignment and the same alignment was further used for the development of a CoMSIA model. The best developed CoMFA model had  $r_{cv}^2 = 0.552$  with six components,  $r_{ncv}^2 = 0.973$ , standard error of estimate = 0.162,  $F$ -value = 281.239, while the best developed CoMSIA model had  $r_{cv}^2 = 0.571$  with six components,  $r_{ncv}^2 = 0.960$ , standard error of estimate = 0.196 and  $F$ -value = 188.701. The predictive  $r^2$  values of these two models showed test set predictions of 0.528 and 0.679 for the best CoMFA and CoMSIA models, respectively. Based on a higher  $r_{pred}^2$  value, the CoMSIA model was found to be the best one. The prediction accuracy and reliability of the best developed CoMSIA model have been validated using well-established methods.

**Electronic supplementary material** The online version of this article (doi:10.1007/s11030-015-9611-5) contains supplementary material, which is available to authorized users.

✉ Mange Ram Yadav  
mryadav11@yahoo.co.in

<sup>1</sup> Pharmacy Department, Faculty of Technology & Engineering, Kalabhavan, The M. S. University of Baroda, Vadodara 390 001, India

Using the inputs from the best CoMSIA contour maps, several novel highly selective peripherally acting CB1 receptor antagonists have been designed and reported herein.

**Keywords** 3D-QSAR · Endocannabinoids · CB1 receptor antagonists · 1,5-Diaryl pyrazole · Rimonabant

## Introduction

The worldwide overweight and obese population in 2012 was 1573 and 520 million, respectively [1], and these numbers are increasing day by day due to lack of sufficient physical work, sedentary life style and consumption of high-fat/energy diet [2–4]. According to WHO, obesity has become the fifth leading risk factor for global deaths. Due to overweight/obesity, at least 2.8 million adults die each year. Elevated body mass index creates a major risk factor for various noncommunicable diseases, such as hypertension, diabetes mellitus, dyslipidemia, osteoarthritis, sleep apnoea and certain types of cancers [5]. Hence, obesity is proving to be a major epidemic health problem facing the human race.

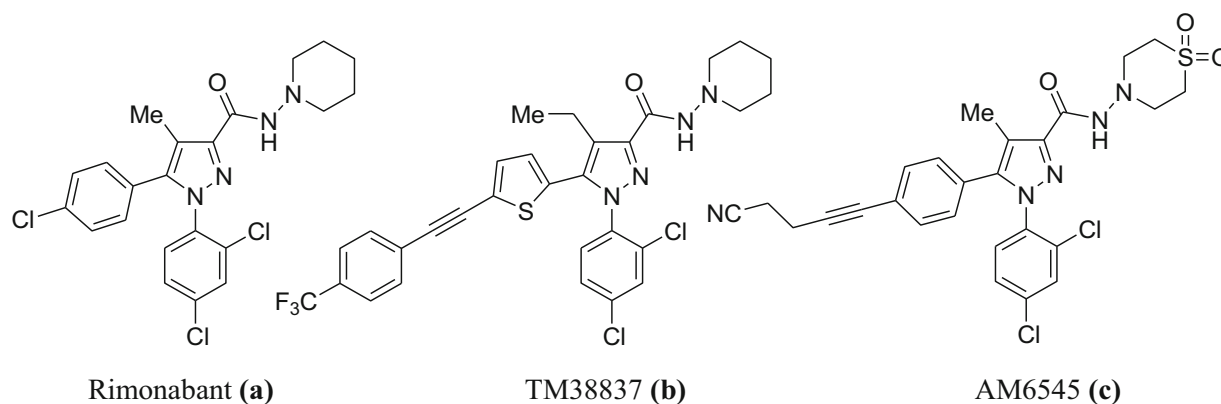
Although a number of targets have been identified for the treatment of obesity, none have proved effective for therapy with effective long-term anti-obesity action and lesser side effects. At present, Orlistat, a gastrointestinal lipase inhibitor, is available in the market for the treatment of obesity having moderate efficacy; however, it presents a number of gastrointestinal adverse effects, such as malabsorption, steatorrhea, flatulence, faecal incontinence, faecal urgency, upset stomach, dyspepsia, abdominal pain and decreased absorption of fat soluble vitamins [4]. In July 2012, Lorcaserin, a selective 5-HT<sub>2C</sub> receptor agonist, received FDA approval for a re-filing application as anti-obesity drug. Initially, Lorcaserin was rejected due to carcinogenicity observed in prelini-

cal studies [6]. The FDA has also approved several drugs such as phentermine, diethylpropion, benzphetamine and phendimetrazine for short-term use for the treatment of obesity. Unfortunately, due to lack of efficacy and presence of several side effects, these drugs could not be proven as ideal drugs for the treatment of obesity [7]. Hence, there remains an unmet need to develop safe and potential drugs for the treatment of obesity.

It is established that the endocannabinoid (EC) system controls food intake and energy homeostasis [8]. Over-activation of the EC system or increased levels of EC are observed in obesity. Thus, blocking the over-activity of the EC system by antagonizing the cannabinoid 1 (CB1) receptors can be considered as the best approach for the treatment of obesity. The CB1 receptors are present in the brain region (e.g., hypothalamus) where they directly regulate orexigenic or anorexigenic signals, and in peripheral tissues, such as testes, eyes, urinary bladder, ileum, adipose tissue, liver, skeletal muscles and pancreas [9]. The energy balance in the body is regulated by peripheral lipogenic mechanisms and the modulation of lipid and carbohydrate metabolism [10, 11]. The therapeutic potential of CB1 receptor antagonists has been extensively explored using rimonabant (**a**), a centrally acting selective CB1 receptor antagonist showing clinical efficacy in weight reduction [12]. The European Commission

they do not get entry into the brain. Neutral compounds, charged compounds and allosteric modulators have also been designed to prevent their entry into the brain, thus avoiding central side effects [4]. By adopting this strategy, we also have been putting our efforts in the design and optimization of compounds as CB1 receptor antagonists with the help of molecular modeling techniques.

A number of researchers are working on the development of peripherally acting CB1 receptor antagonists. Most of these efforts have focused on the design of 1,5-diaryl pyrazole derivatives similar to rimonabant [15]. 7TM Pharma discovered diaryl pyrazole TM38837 (**b**), a peripherally acting CB1 receptor antagonists which showed a brain-to-plasma ratio of 1:33 [16]. The data suggested that a 100-mg dose of TM38837 did not show any central nervous system (CNS) side effects as it did not enter into the brain [17]. Similarly, AM6545 (**c**), a diaryl pyrazole derivative, offered very promising results as peripheral CB1 receptor antagonist [18]. Recently, an exhaustive review on centrally and peripherally acting CB1 receptor antagonists has been published covering the detailed development process of different classes of peripherally acting compounds from centrally acting CB1 receptor antagonists. The review gives emphasis to the design of peripherally acting CB1 receptor antagonists to minimize CNS side effects [15].



had approved rimonabant in 2006 as an anti-obesity agent. Unfortunately, it was withdrawn from the market in 2008 due to its psychiatric side effects including depression, anxiety, irritability, suicidal tendency, gastrointestinal disorders (e.g., nausea) and neurological alterations (e.g., headache vertigo) [13, 14]. Later on, researchers shifted their focus to alternative strategies which could lead to reduction in the side effects shown by rimonabant. Thus, emphasis was given to design non-brain-penetrating or peripherally acting selective CB1 receptor antagonists that do not cross into the BBB thereby reducing the psychiatric side effects. Efforts were made to increase the polar surface area (PSA) and decrease the lipophilicity to make the compounds more polar so that

Computer-aided drug designing (CADD) techniques are playing an important role in the drug discovery process and optimization of lead compounds [19, 20]. Three-dimensional quantitative structure–activity relationship (3D-QSAR) is one of the rational drug design approaches that is being successfully utilized for the development of potent bioactive compounds. Our laboratory has been actively engaged in designing potential enzyme inhibitors with the help of CADD techniques [21–33]. In this present work, we report a highly predictive 3D-QSAR model for peripherally acting selective CB1 receptor antagonists containing the 1,5-diaryl pyrazole scaffold. Recently, Hernandez-Vazquez et al. [34] reported 3D-QSAR studies on pyrazole derivatives acting

as CB1 receptor antagonists. However, in this study, only centrally acting CB1 receptor antagonists were considered. To design peripherally acting CB1 receptor antagonists, one needs to know the structural requirements responsible for such an activity. There is an unmet need for peripherally acting CB1 receptor antagonists that have high potency and minimal side effects for the treatment of obesity. Herein, we report the development of a highly predictive 3D-QSAR model for peripherally acting CB1 receptor antagonists. For the present study, a series of peripherally acting 1,5-diaryl pyrazoles have been selected. The main objective behind this work is to identify the important structural features required for the antagonistic activity of the peripherally acting compounds using 3D-QSAR techniques and use this information for the design of more potent and selective compounds.

## Material and methods

### Dataset

A dataset of peripherally acting selective CB1 receptor antagonists was chosen for the present 3D-QSAR study. A total of 72 compounds containing the 1,5-diaryl pyrazole scaffold having CB1 receptor antagonistic activity were chosen [35,36]. Compounds with same range of biological activity and those having structural similarity were omitted from the dataset. The compounds which did not have biological activity in the exact numerical form were also removed from the dataset. CB1 receptor antagonistic activity was reported in terms of  $IC_{50}$  values in the nanomolar (nM) range. These  $IC_{50}$  values were converted into their corresponding  $pIC_{50}$  ( $-\log IC_{50}$ ) which were utilized as dependent variables for the development of both CoMFA and CoMSIA models. The structures and biological activity of the compounds used are shown in Table 1.

### Distribution of training and test set

The compounds of the dataset were distributed into the training set (54 compounds) and test set (18 compounds) in an appropriate 3:1 ratio as shown in Table 1. The compounds in the training and test sets were divided randomly by applying the following logic: (i) a wide range of biological activity and structural variations which were present in the training set were also maintained in the test set. (ii) The template molecule (the most potent compound among the dataset) was made a part of the training set. The predictability of the models was assessed using the test set compounds. The activities of the training set and test set ranged from 0.1 nM ( $pIC_{50} = 10.000$ ) to 980 nM ( $pIC_{50} = 6.009$ ) and 0.8 nM ( $pIC_{50} = 9.097$ ) to 455 nM ( $pIC_{50} = 6.342$ ), respectively.

### Molecular modeling

Molecular modeling studies were carried out using the SYBYL 7.0 molecular modeling software from Tripos, Inc. [37]. The 'Sketch Molecule' module of SYBYL 7.0 was used to build the 3D structures of the molecules. Conjugate gradient and steepest descent methods were used for energy minimization using the Tripos force field and Gasteiger–Huckel charges until a root mean square deviation (RMSD) of 0.001 and 0.05 kcal/mol, respectively, were achieved. The energy minimization procedure was carried out using a nonbonded interaction cut-off of 8.0 Å, having a distance-dependent dielectric function with dielectric constant of 1.0. Thus, conformers having the lowest energy generated by the above-said two methods were used for the alignments. A conformational search for all the compounds was also carried out by a simulated annealing technique with the Tripos force field in SYBYL. The molecules were heated to 700 K followed by cooling to 300 K and the time spent for annealing was 1000 fs. The time increment for dynamics calculations was 0.5 fs and the coupling time for temperature regulation was 2.0 fs. Ten consecutive cycles were performed. Further, a conjugate gradient method was used to minimize the lowest energy conformers using the Tripos force field until a RMSD of  $0.001 \text{ kcal mol}^{-1} \text{ Å}$  was achieved [24]. The conformational strain energy of all the compounds is shown in Table 1.

### Alignment rules

To obtain the best 3D-QSAR models with high predictive accuracy, the proper alignment of all the structures is essential because the results of CoMFA and CoMSIA studies are alignment sensitive. Thus, the molecular alignment of the 3D structures plays a vital role in CoMFA and CoMSIA analysis [38]. The most potent compound (**20**) in the series was used as the template molecule for alignment purposes. We also developed 3D-QSAR models with two equipotent compounds (**3** and **24**) as templates using different types of alignments. Unfortunately, poorer statistical results were obtained for these models when compared to the model developed using compound (**20**) as template. The range of  $r_{cv}^2$  values was 0.294–0.412 having an optimum number of component (ONC) value of 2; also  $r_{ncv}^2$  values at ONC = 2 were not in the acceptable range for the models developed using compounds (**3** and **24**). The results obtained for the model developed using compound (**20**) as template were encouraging, i.e., ( $r_{cv}^2 = 0.552$  with ONC = 6). Thus, compound (**20**) was selected as the template molecule for further studies. The molecular alignments of the compounds were carried out using different methods, such as atom-based, data-based, centroid-based, centroid/atom-based as shown in Fig. 1.

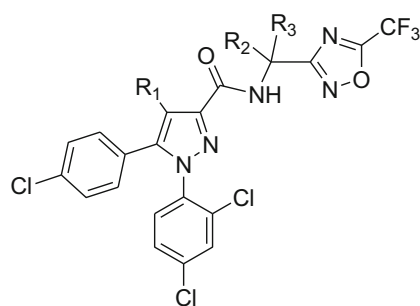
**Table 1** Chemical structures of compounds (1–72) and their biological activities

(1-18)

| Compd | R <sub>1</sub>                   | R <sub>2</sub> | R <sub>3</sub> | Strain energy | Experimental          |                          | Predicted <i>pIC</i> <sub>50</sub> |        |
|-------|----------------------------------|----------------|----------------|---------------|-----------------------|--------------------------|------------------------------------|--------|
|       |                                  |                |                |               | IC <sub>50</sub> (nM) | <i>pIC</i> <sub>50</sub> | CoMFA                              | CoMSIA |
| 1*    | Cl                               | Me             |                | 3.22          | 145                   | 6.839                    | 7.826                              | 7.729  |
| 2     | Cl                               | Et             |                | 2.10          | 0.5                   | 9.301                    | 9.788                              | 9.724  |
| 3     | Br                               | Et             |                | 0.97          | 0.1                   | 10.000                   | 9.777                              | 9.828  |
| 4     | OSO <sub>2</sub> <sup>n</sup> Pr | Me             |                | 4.48          | 1.1                   | 8.959                    | 8.850                              | 9.021  |
| 5*    | CN                               | Et             |                | 0.87          | 22                    | 7.658                    | 7.556                              | 8.016  |
| 6     | OMe                              | Et             |                | 2.07          | 5                     | 8.301                    | 8.325                              | 8.460  |
| 7     | CO <sub>2</sub> Et               | Et             |                | 3.02          | 17                    | 7.770                    | 7.634                              | 7.797  |
| 8     | Cl                               | Me             |                | 2.96          | 15                    | 7.824                    | 7.764                              | 7.763  |
| 9*    | Cl                               | Me             |                | 4.12          | 2                     | 8.699                    | 7.925                              | 8.361  |

Table 1 continued

|     |    |    |  |      |    |       |       |       |
|-----|----|----|--|------|----|-------|-------|-------|
| 10  | Cl | Me |  | 3.96 | 22 | 7.658 | 7.717 | 7.383 |
| 11  | Cl | Me |  | 4.26 | 10 | 8.000 | 8.046 | 7.833 |
| 12* | Cl | Me |  | 0.51 | 12 | 7.921 | 7.891 | 8.021 |
| 13  | Cl | Me |  | 6.54 | 11 | 7.959 | 7.896 | 7.698 |
| 14  | Cl | Me |  | 5.93 | 88 | 7.056 | 7.131 | 6.988 |
| 15  | Cl | Me |  | 8.42 | 63 | 7.201 | 7.280 | 7.359 |
| 16  | Cl | Me |  | 1.60 | 33 | 7.481 | 7.415 | 7.480 |
| 17  | Cl | Me |  | 3.46 | 3  | 8.523 | 8.803 | 8.316 |
| 18  | Cl | Me |  | 3.32 | 6  | 8.222 | 8.317 | 8.324 |



(19-25)

| Compd | R <sub>1</sub>      | R <sub>2</sub>                                     | R <sub>3</sub> | Strain energy | Experimental          |                   | Predicted |        |
|-------|---------------------|--|----------------|---------------|-----------------------|-------------------|-----------|--------|
|       |                     |  |                |               | IC <sub>50</sub> (nM) | pIC <sub>50</sub> | CoMFA     | CoMSIA |
| 19*   | Me                  | Et   | Me             | 3.39          | 6                     | 8.222             | 8.304     | 8.118  |
| 20    | Me                  | -CH <sub>2</sub> CH <sub>2</sub> -                 | Me             | 2.27          | 0.1                   | 10.000            | 9.774     | 9.751  |
| 21*   | Me                  | -CH <sub>2</sub> CH <sub>2</sub> CH <sub>2</sub> - | Me             | 0.42          | 0.8                   | 9.097             | 9.229     | 9.516  |
| 22    | CH <sub>2</sub> OH  | Me   | Me             | 4.40          | 0.4                   | 9.398             | 9.097     | 9.336  |
| 23*   | CH <sub>2</sub> OMe | Me   | Me             | 4.70          | 4                     | 8.398             | 8.750     | 8.895  |
| 24    | CH <sub>2</sub> OH  | -CH <sub>2</sub> CH <sub>2</sub> -                 | Me             | 2.36          | 0.1                   | 10.000            | 10.246    | 10.157 |
| 25    | CO <sub>2</sub> Et  | -CH <sub>2</sub> CH <sub>2</sub> -                 | Me             | 6.84          | 1                     | 9.000             | 9.002     | 8.809  |

Table 1 continued

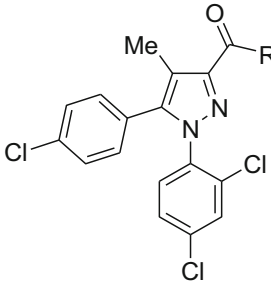
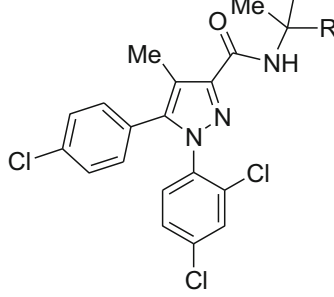
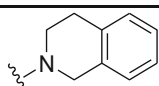
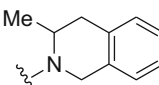
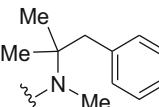
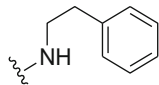
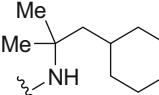
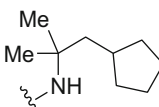
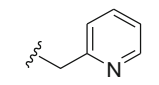
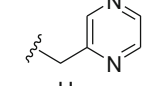
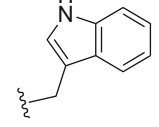
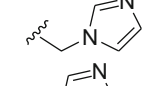
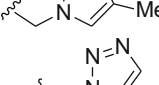
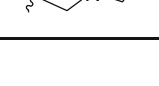
| <div style="display: flex; justify-content: space-around; align-items: center;"> <div style="text-align: center;">  <p>(26-31)</p> </div> <div style="text-align: center;">  <p>(32-56)</p> </div> </div> |   |               |                |            |           |            |
|--|---|---------------|----------------|------------|-----------|------------|
| Compd  | R   | Strain energy | Experimental   |            | Predicted | $pIC_{50}$ |
|  |   |               | $IC_{50}$ (nM) | $pIC_{50}$ | CoMFA     |            |
| 26   |    | 0.31          | 18             | 7.745      | 7.722     | 7.828      |
| 27   |    | 3.66          | 20             | 7.699      | 7.743     | 7.636      |
| 28   |    | 5.55          | 96             | 7.018      | 7.159     | 7.077      |
| 29   |   | 1.75          | 10             | 8.000      | 8.167     | 7.696      |
| 30   |  | 3.82          | 26             | 7.585      | 7.611     | 7.529      |
| 31   |  | 0.61          | 21             | 7.678      | 7.714     | 7.556      |
| 32   |  | 2.59          | 2              | 8.699      | 8.671     | 8.799      |
| 33   |  | 2.08          | 57             | 7.244      | 7.330     | 7.454      |
| 34   |  | 4.92          | 20             | 7.699      | 7.570     | 7.748      |
| 35   |  | 4.24          | 71             | 7.149      | 7.178     | 7.247      |
| 36   |  | 3.05          | 20             | 7.699      | 7.526     | 7.587      |
| 37*  |  | 3.25          | 15             | 7.822      | 7.608     | 7.788      |

Table 1 continued

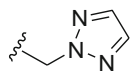
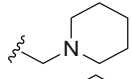
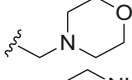
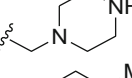
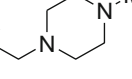
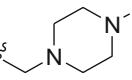
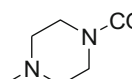
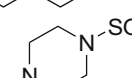
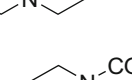
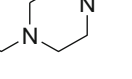
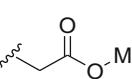
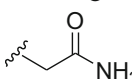
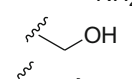
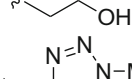
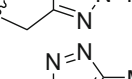
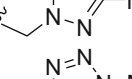
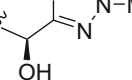
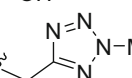
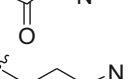
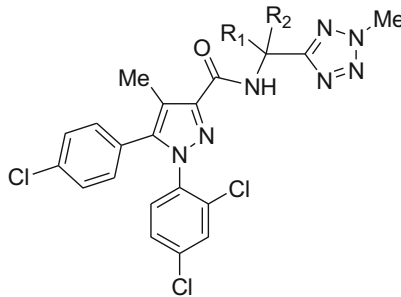
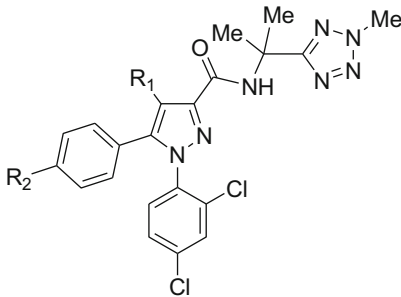
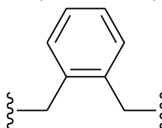
|     |   |      |     |       |       |       |
|-----|---|------|-----|-------|-------|-------|
| 38* |    | 0.69 | 16  | 7.796 | 7.434 | 7.685 |
| 39* |    | 6.62 | 455 | 6.342 | 6.714 | 6.635 |
| 40  |    | 1.16 | 47  | 7.328 | 7.129 | 7.385 |
| 41  |    | 1.43 | 900 | 6.046 | 6.212 | 6.019 |
| 42* |    | 1.67 | 310 | 6.509 | 6.554 | 6.328 |
| 43  |    | 0.59 | 855 | 6.068 | 6.222 | 6.176 |
| 44  |    | 2.25 | 633 | 6.199 | 6.253 | 6.205 |
| 45  |    | 3.25 | 980 | 6.009 | 5.829 | 5.892 |
| 46  |    | 2.64 | 29  | 7.538 | 7.416 | 7.463 |
| 47  |    | 1.37 | 17  | 7.770 | 7.705 | 7.647 |
| 48  |   | 0.72 | 25  | 7.602 | 7.612 | 7.721 |
| 49* |  | 0.73 | 60  | 7.222 | 7.825 | 7.831 |
| 50* |  | 2.30 | 33  | 7.481 | 8.014 | 7.684 |
| 51  |  | 2.38 | 71  | 7.149 | 7.237 | 7.416 |
| 52  |  | 2.66 | 18  | 7.745 | 7.874 | 7.805 |
| 53  |  | 7.73 | 74  | 7.131 | 7.044 | 7.168 |
| 54* |  | 2.48 | 6   | 8.222 | 8.303 | 7.520 |
| 55  |  | 5.04 | 11  | 7.959 | 7.901 | 8.094 |
| 56  |  | 2.27 | 88  | 7.056 | 7.276 | 7.299 |

Table 1 continued

| <div>  <p>(57-64)</p> </div> |  |                                  |                  | <div>  <p>(65-72)</p> </div> |                           |           |                           |
|---|--|----------------------------------|------------------|--|---------------------------|-----------|---------------------------|
| Compd   | R <sub>1</sub>   | R <sub>2</sub>                   | Strain<br>energy | Experimental   |                           | Predicted | <i>p</i> IC <sub>50</sub> |
|   |  |                                  |                  | IC <sub>50</sub> (nM)  | <i>p</i> IC <sub>50</sub> | CoMFA     |                           |
| 57  | H  | H                                | 0.09             | 100  | 7.000                     | 7.104     | 7.286                     |
| 58*   | -CH <sub>2</sub> CH <sub>2</sub> -   |                                  | 0.11             | 61   | 7.215                     | 8.517     | 7.846                     |
| 59  | Et   | Et                               | 6.34             | 35   | 7.456                     | 7.250     | 7.569                     |
| 60  | -CH <sub>2</sub> CH <sub>2</sub> CH <sub>2</sub> -                                 |                                  | 0.57             | 10   | 8.000                     | 7.944     | 7.966                     |
| 61*   | Me   | Et                               | 3.79             | 18   | 7.745                     | 7.900     | 7.303                     |
| 62*   | Me   | -CH <sub>2</sub> OH              | 2.51             | 77   | 7.114                     | 7.177     | 7.288                     |
| 63  | -(CH <sub>2</sub> CH <sub>2</sub> ) <sub>2</sub> -                                 |                                  | 0.42             | 16   | 7.799                     | 7.796     | 7.896                     |
| 64  |  |                                  | 0.70             | 14   | 7.854                     | 7.758     | 7.960                     |
| 65*   | Et   | Br                               | 0.23             | 4  | 8.398                     | 8.871     | 8.255                     |
| 66  | Me   | OSO <sub>2</sub> <sup>n</sup> Pr | 2.94             | 7  | 8.155                     | 8.239     | 8.415                     |
| 67  | Me   | CN                               | 1.90             | 31   | 7.509                     | 7.494     | 7.382                     |
| 68  | Et   | CN                               | 2.07             | 34   | 7.469                     | 7.627     | 7.463                     |
| 69  | CH <sub>2</sub> OH   | Cl                               | 2.52             | 8  | 8.097                     | 8.104     | 8.343                     |
| 70  | CH <sub>2</sub> F  | Cl                               | 2.39             | 3  | 8.523                     | 8.164     | 7.850                     |
| 71  | CO <sub>2</sub> Et   | Cl                               | 6.75             | 1  | 9.000                     | 8.937     | 8.879                     |
| 72  | CH <sub>2</sub> OH   | OSO <sub>2</sub> <sup>n</sup> Pr | 4.77             | 0.5  | 9.301                     | 9.245     | 9.118                     |

\* Test set compounds

### Atom-based alignment

In this alignment, selected atoms of the template molecule (**20**) were used for RMS fitting over the corresponding atoms of all the compounds in the dataset. Two types of alignments (I–II) were performed using different atoms as shown in Fig. 1.

### Centroid-based alignment

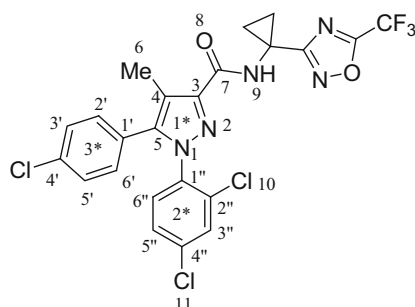
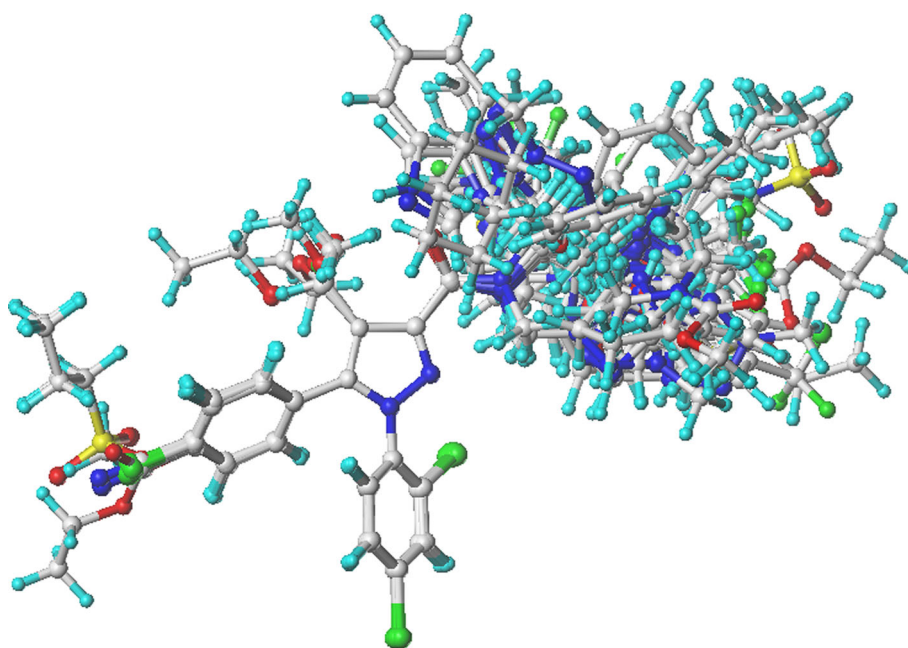
In this alignment, the pyrazole ring and the two phenyl rings were defined as centroids (Fig. 1). Pairwise superimposition

of centroids of template molecule (**20**) was carried out with the corresponding centroids of all the compounds (alignment III).

### Centroid/atom-based alignment

In this alignment, both centroids and atoms were considered for the purpose of alignment. Two types of alignments (IV–V) were defined (Fig. 1). Pairwise superimposition of centroids and atoms was done in this alignment.



**Fig. 1** Template molecule (**20**) and the alignment rules**Fig. 2** Alignment of the compounds using data-based alignment (VI). (Color figure online)

### Data-based alignment

Data-based alignment was carried out using the 'Align Database' function in SYBYL. Different types of common fragments used for data-based alignment (VI–X) are shown in Fig. 1. All the compounds were aligned to these common fragments. Aligned compounds with the best fragments are shown in Fig. 2.

### CoMFA and CoMSIA interaction energy calculations

In the CoMFA analysis, the steric (S) and electrostatic (E) fields were calculated by applying regular space grid of 2.0 Å at each lattice intersection in all the three dimensions within the defined region. Standard Tripos force field was used for S and E fields. An  $sp^3$  carbon atom was used as a probe atom with +1.0 charge and distance-dependent dielectric constant of 1.00. The S and E fields of CoMFA analysis were truncated

at +30.0 kcal/mol [25,39,40]. In the CoMSIA analysis, the interaction energy was calculated using five potential fields, namely the S, E, hydrophobic (H), hydrogen bond acceptor (A) and hydrogen bond donor (D) at each lattice intersection of a regular space grid of 2.0 Å. The radius of the probe atom was 1.0 Å and +1.0 charge with +1.0 hydrophobicity, +1.0 D and +1.0 A were used for the CoMSIA analysis. The contribution from all the descriptors was truncated at 0.3 kcal/mol [25,41].

### Partial least square (PLS) analysis

To develop our 3D-QSAR models, PLS analysis was used to linearly correlate biological activity ( $pIC_{50}$ ) as the dependent variable with CoMFA and CoMSIA descriptors as the independent variables. To assess the internal predictive accuracy of the models, a cross-validation was performed using the leave-one-out method. In this method, one compound

**Table 2** Summary of CoMFA results

| Statistical parameters | Types of alignment |        |         |         |         |                |         |         |         |         |
|------------------------|--------------------|--------|---------|---------|---------|----------------|---------|---------|---------|---------|
|                        | I                  | II     | III     | IV      | V       | VI             | VII     | VIII    | IX      | X       |
| $r_{cv}^2$             | 0.381              | 0.421  | 0.424   | 0.423   | 0.461   | <b>0.552</b>   | 0.542   | 0.546   | 0.522   | 0.561   |
| ONC                    | 3                  | 2      | 5       | 6       | 6       | <b>6</b>       | 5       | 6       | 5       | 6       |
| SEP                    | 0.757              | 0.744  | 0.738   | 0.747   | 0.722   | <b>0.658</b>   | 0.658   | 0.662   | 0.672   | 0.651   |
| $r_{ncv}^2$            | 0.848              | 0.743  | 0.940   | 0.972   | 0.955   | <b>0.973</b>   | 0.945   | 0.964   | 0.943   | 0.974   |
| SEE                    | 0.376              | 0.486  | 0.238   | 0.164   | 0.209   | <b>0.162</b>   | 0.228   | 0.187   | 0.233   | 0.158   |
| <i>F</i> -value        | 92.792             | 73.842 | 150.156 | 271.783 | 164.924 | <b>281.239</b> | 164.613 | 207.441 | 157.391 | 296.518 |
| $Pr^2 = 0$             | 0                  | 0      | 0       | 0       | 0       | <b>0</b>       | 0       | 0       | 0       | 0       |
| $r_{pred}^2$           | 0.492              | 0.467  | 0.330   | 0.438   | 0.402   | <b>0.528</b>   | 0.501   | 0.464   | 0.454   | 0.416   |

Bold values represent best results

was removed at a time from the dataset and its activity was predicted by the developed model from the rest of the compounds in the dataset. The cross-validated correlation coefficient ( $r_{cv}^2$ ) (Eq. 1) and ONCs were obtained by this method. Using the ONC, the non-cross-validated correlation coefficient ( $r_{ncv}^2$ ) and standard error of estimation (SEE) were calculated to evaluate the fitting quality of the models [42–44].

$$r_{cv}^2 = 1 - \frac{\sum (Y_{\text{predicted}} - Y_{\text{actual}})^2}{\sum (Y_{\text{actual}} - Y_{\text{mean}})^2}, \quad (1)$$

where  $Y_{\text{predicted}}$  is the predicted value of the target property ( $pIC_{50}$ ),  $Y_{\text{actual}}$  is the actual value of the target property ( $pIC_{50}$ ) and  $Y_{\text{mean}}$  is the mean value of the target property ( $pIC_{50}$ ).

### Predictive ability of CoMFA and CoMSIA models

The predictive accuracy of the derived CoMFA and CoMSIA models was calculated with the test set compounds expressed as  $r_{pred}^2$  using the following equation (Eq. 2):

$$r_{pred}^2 = (SD - PRESS)/SD, \quad (2)$$

where

$SD = \sum [(target\ data\ value) - (target\ data\ mean)]^2$ , and

$PRESS = \sum [(target\ data\ value) - (corresponding\ predicted\ data\ value)]^2$ .

SD is defined as the sum of the squared deviations between the biological activities of the test set molecules and the mean activity of the training set compounds, whereas PRESS is defined as the sum of the squared deviation between the observed and the predicted activities of the test set compounds [45].

## Results and discussion

The present work was carried out with the aim to develop the best predictive 3D-QSAR model for peripherally acting 1,5-diaryl pyrazole-containing CB1 receptor antagonists. Both CoMFA and CoMSIA methods were used for the development of QSAR models. A set of 72 compounds having peripherally CB1 receptor antagonistic activity was used for this study (Table 1). The most potent compound (**20**) served as the template molecule for the alignment process.

### CoMFA analysis

Peripherally acting 1,5-diaryl pyrazole-containing CB1 receptor antagonists were utilized for the development of 3D-QSAR models with different fields of CoMFA and CoMSIA methods. A number of models were developed by applying various alignments (Figs. 1, 2). The result of these different alignments is summarized in Table 2. A QSAR model can be judged for its credible prediction of biopotency of unknown molecules on the basis of statistical parameters. All the necessary statistical parameters, such as  $r_{ncv}^2$ ,  $r_{cv}^2$ , SEE, standard error of prediction (SEP), Fischer statistics (*F*-test), number of components and predictive correlation coefficient were analyzed for the evaluation of the predictive accuracy of the developed 3D-QSAR models.

To obtain the best model, various alignments, such as two types of atom-based (I and II), one type of centroid-based (III), two types of centroid/atom-based (IV and V) and five types of data-based alignments (VI–X) were used. Out of these alignments, the data-based (VI) alignment resulted in the best model. Alignment (VI) afforded  $r_{cv}^2 = 0.552$  with six components,  $r_{ncv}^2 = 0.973$ , *F*-value = 281.239 and  $r_{pred}^2 = 0.528$ . The remaining CoMFA results of different alignments are shown in Table 2. It was observed that data-based alignment (VI) offered the best statistical parameters showing high  $r_{cv}^2$ ,  $r_{ncv}^2$ , *F*-value, low SEE value and good

**Table 3** Summary of CoMSIA results

| Statistical parameters | Combination of fields used |         |         |                |         |         |         |         |
|------------------------|----------------------------|---------|---------|----------------|---------|---------|---------|---------|
|                        | SHE                        | SED     | SEA     | SHA            | HAD     | SEHA    | SEHD    | SEHDA   |
| $r_{cv}^2$             | 0.683                      | 0.518   | 0.467   | <b>0.571</b>   | 0.476   | 0.537   | 0.645   | 0.529   |
| ONC                    | 6                          | 6       | 5       | <b>6</b>       | 6       | 6       | 6       | 6       |
| SEP                    | 0.553                      | 0.518   | 0.695   | <b>0.644</b>   | 0.712   | 0.669   | 0.586   | 0.674   |
| $r_{ncv}^2$            | 0.954                      | 0.952   | 0.919   | <b>0.960</b>   | 0.945   | 0.963   | 0.956   | 0.966   |
| SEE                    | 0.210                      | 0.215   | 0.277   | <b>0.196</b>   | 0.231   | 0.189   | 0.206   | 0.181   |
| <i>F</i> -value        | 163.620                    | 156.235 | 108.747 | <b>188.701</b> | 134.174 | 203.463 | 173.098 | 223.662 |
| $Pr^2 = 0$             | 0                          | 0       | 0       | <b>0</b>       | 0       | 0       | 0       | 0       |
| $r_{pred}^2$           | 0.437                      | 0.354   | 0.470   | <b>0.679</b>   | 0.510   | 0.429   | 0.386   | 0.367   |

Bold values represent best results

$r_{pred}^2$ . Thus, data-based alignment (VI) was considered to be the best model on the basis of its predictive accuracy. Contributions of S and E fields for the best developed model were 43.4 and 56.6 %, respectively.

### CoMSIA analysis

The CoMSIA method is used for overcoming the limitations of S and E fields of the CoMFA method. The CoMSIA method is a combination of five different fields, including S, E, H, D and A. Using these different combinations of fields, various CoMSIA models were developed that showed moderate to high internal and external predictivity as shown in Table 3. The CoMSIA model obtained with a combination of all the fields yielded  $r_{cv}^2 = 0.529$  with six components,  $r_{ncv}^2 = 0.966$ , *F*-value = 223.662 and  $r_{pred}^2 = 0.367$ . The contributions of all SEHDA fields for this model were 11.2, 37.1, 20.9, 8.9 and 21.9 %, respectively. The best CoMSIA model developed using a combination of SHA fields yielded  $r_{cv}^2 = 0.571$  with six components,  $r_{ncv}^2 = 0.960$ , *F*-value = 188.701 and  $r_{pred}^2 = 0.679$ . The contributions of SHA fields were 19.9, 39.9 and 40.3 %, respectively. Figures 3 and 4 represent graphs plotted between the experimental and predicted

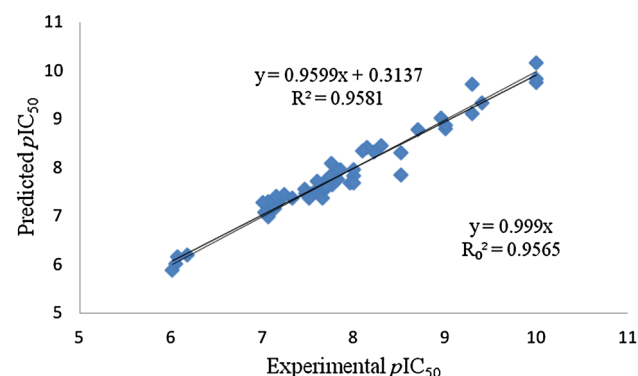


**Fig. 3** Graph of experimental versus predicted activities of training set of compounds for the best CoMSIA model

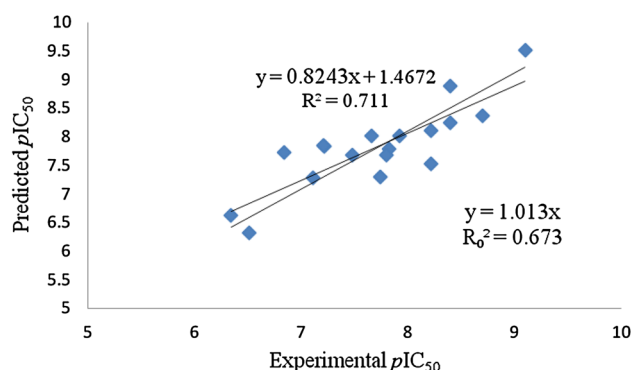


**Fig. 4** Graph of experimental versus predicted activities of the test set compounds for the best CoMSIA model

activities for the respective training set and test set compounds for the best developed CoMSIA model (SHA). The best developed CoMFA model considered the S and E interactions only showing an acceptable  $r_{cv}^2$  value of 0.552 and  $r_{pred}^2 = 0.528$ . However, the best developed CoMSIA (SHA) model yielded higher  $r_{cv}^2$  value of 0.571 and  $r_{pred}^2 = 0.679$ , indicating that CoMSIA (SHA) model is a better predictive model.

### Validation of the best CoMSIA model

Validation of a developed model is an important criterion if the developed model is to be used for prediction purposes. Different validation parameters, such as internal validation, *F*-test, *Y*-randomization test, bootstrapping, external validation and modified  $r^2$  ( $r_m^2$ ) were utilized to validate the best developed CoMSIA model.

### Internal validation

To corroborate the predictive accuracy of the model and its ability to reproduce biological activity of the compounds for the training set [46], an internal validation was per-

**Table 4** Summary of *Y*-randomization test for the best CoMSIA (SHA) model

| Parameters  | Values          |
|---|-----------------|
| Number of random trials   | 10              |
| Number of trials with $r_{cv}^2$ and $r_{ncv}^2$ greater than non-random trials | 0               |
| Number of trials with $r_{cv}^2$ and $r_{ncv}^2$ lesser than non-random trials  | 10              |
| Range of $r_{ncv}^2$ from randomized data                                       | 0.301 to 0.580  |
| Range of $r_{cv}^2$ from randomized data  | −0.693 to 0.021 |

formed. The best CoMSIA model (SHA) showed a good cross-validated correlation ( $r_{cv}^2 = 0.571$ ,  $r_{ncv}^2 = 0.960$ ). These results indicate that the developed model has a high internal predictive accuracy.

### Fischer statistics (*F*-test)

Fischer value (*F*) is defined as the ratio between the explained and unexplained variance for a given number of degrees of freedom. A higher *F*-value for the developed model than the threshold tabulated value indicates that there is a high probability of the developed model to be statistically significant [47]. The *F*-value for the best CoMSIA model (SHA) was 188.701 [ $F_{05}(6, 71) = 2.22$  (Tab)] at 95 % confidence level, indicating that the model is statistically significant.

### *Y*-randomization test

The *Y*-randomization test is the most commonly used test to eliminate the possibility of chance correlation and ensure the robustness of the developed model [25, 48]. This test is performed by randomly shuffling the dependent variable vector ( $pIC_{50}$ ) and using the previously selected independent variable matrix (descriptors) of the training set compounds followed by building the model using the original alignment rule and testing the model by predicting the biological activity of the training and test set compounds. It is expected that the derived model would show significantly lower  $r_{cv}^2$  and  $r_{ncv}^2$  values than the original one after several repetition trials [25]. Ten random trials were performed for the best developed CoMSIA (SHA) model, and the poor  $r_{cv}^2$  and  $r_{ncv}^2$  values obtained ensured the robustness of the original model. The non-cross-validated and cross-validated  $r^2$  for the CoMSIA (SHA) model were obtained in the range of 0.301 to 0.580 and −0.693 to 0.021, respectively, as shown in Table 4. Thus, the random trials were not matching with the original model. Hence, *Y*-randomization test validates that the original model is not a case of chance correlation.

### Bootstrapping

Validation with bootstrapping was carried out for 100 runs to further assess the robustness and statistical confidence of the developed model. In the bootstrapping method, many new datasets were generated from the original dataset by randomly selecting samples from the original dataset and the model is generated using the same (6) optimal number of components. Each of these bootstrapping samples is used for performing statistical calculations. The measurement of bias of the original calculations is based on the difference between the calculated parameters from the original dataset and the average of the parameters calculated from the many bootstrapping samplings [49]. For the best CoMSIA model (SHA), the bootstrapped variance value ( $r_{bs}^2 = 0.977$ ) and bootstrapped standard deviation ( $SD_{bs} = 0.008$ ) suggest a good internal consistency within the dataset. This confirms that a reliable and stable 3D-QSAR model has been successfully developed.

### External validation

The predictive performance of a model is evaluated via an external validation using test set compounds. A set of 18 compounds were used for the external validation of the developed CoMFA/CoMSIA models to verify the stability and prediction accuracy of the developed models. The predictive correlation coefficient  $r_{pred}^2$  values were 0.528 and 0.679 for CoMFA and CoMSIA (SHA) models, respectively.

### Modified $r^2$ ( $r_m^2$ )

Modified  $r_m^2$  is another validation criterion to validate the external predictability of developed QSAR models. The  $r_m^2$  value is used to penalize a model containing a large difference between the actual and the predicted activities of the test set. The predicted activity of test set compounds should be near to the corresponding actual activity of the compounds; hence, the  $r_0^2$  value will be close to the  $r^2$  value in the case of a good prediction. For the best external prediction case, the  $r_m^2$  value will be similar to the  $r^2$  value ( $r_m^2 = r^2$ ) while in the worst condition, the value of  $r_m^2$  will be zero ( $r_m^2 = 0$ ). The external predictability of a model is considered to be good when the  $r_m^2$  value is greater than 0.5. The best developed CoMSIA (SHA) model exhibited  $r_m^2$  values of 0.920 and 0.575 for training and test set, respectively, indicating that the developed model was highly predictive and reliable. The  $r_m^2$  value can be calculated using Eq. 3 [50, 51].

$$r_m^2 = r^2 \left( 1 - \sqrt{|r^2 - r_0^2|} \right). \quad (3)$$

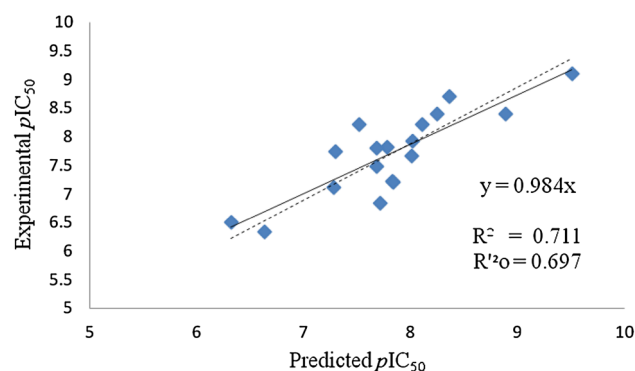


**Fig. 5** Graph of predicted versus experimental activities of the test set compounds for the best CoMSIA model

### Tropsha's validation tests

According to Tropsha [52,53], a good model should pass the following criteria:  $q^2 > 0.5$ ,  $r^2 > 0.6$ ,  $[(R^2 - R_0^2)/R^2] < 0.1$  or  $[(R^2 - R_0^2)/R^2] < 0.1$  and  $0.85 \leq k \leq 1.15$  or  $0.85 \leq k' \leq 1.15$ . The best CoMSIA model (SHA) showed higher cross-validated  $r^2$  ( $q^2 = 0.571$ ) which is generally considered as a reliable parameter for a good predictive QSAR model. The predicted  $r^2$  value of the best CoMSIA model (SHA) was 0.679. Next parameter  $[(R^2 - R_0^2)/R^2] < 0.1$  or  $[(R^2 - R_0^2)/R^2] < 0.1$  indicates that at least one of the correlation coefficient for regression line passing through the origin  $R_0^2$  or  $R_0'^2$  should be close to  $R^2$ .  $[(R^2 - R_0^2)/R^2]$  and  $[(R^2 - R_0'^2)/R^2]$  values are observed as 0.0534 and 0.0197, respectively, which are less than 0.1 signifying a good QSAR model. The fourth parameter  $0.85 \leq k \leq 1.15$  or  $0.85 \leq k' \leq 1.15$  indicates that at least one slope of the regression lines passing through the origin should be close to one. The regression plots of experimental versus predicted activities and predicted versus experimental activities were constructed as shown in Figs. 4 and 5. The  $k$  and  $k'$  values are observed to be 1.103 and 0.984, respectively, which are in the given range. Thus, all the validation parameters satisfy the above-mentioned criteria suggesting that the developed model is a reliable one.

### Domain of applicability

It is not possible for any QSAR model, even if it is robust and validated, to predict the exact activity of the entire universe of chemicals. The domain of applicability defines the predictions for only those compounds to be reliable that fall into the domain. Domain of applicability is calculated using both similarity measurements and leverages.

The first method, similarity measurement, is based on the Euclidean distances among all training and test set compounds for defining the domain of applicability of the models. The distance of a test compound to its nearest neighbour in

the training set was compared to the predefined applicability domain (APD) threshold. If the distance is higher than APD, the prediction is considered unreliable. APD can be calculated using Eq. (4)

$$\text{APD} = \langle d \rangle + Z\sigma, \quad (4)$$

where  $\langle d \rangle$  and  $\sigma$  are average and standard deviation of all distances and  $Z$  is the empirical cut-off value.

The second method is based on the calculation of the leverage  $h_i$  for each chemical, which can be calculated using Eq. (5).

$$h_i = x_i^T (X^T X)^{-1} x_i, \quad (5)$$

where  $x_i$  is the descriptor row vector of the query compound and  $X$  is the  $k \times n$  matrix containing  $k$  values for each one of the  $n$  training compounds. If the leverage value is greater than  $3k/n$ , then it is considered too large to be reliable, indicating that the predicted response is the result of substantial extrapolation of the model [53–55].

Applicability of domain was performed by using *Enalos KNIME nodes* (<http://www.novamechanics.com/knime.php>) [53]. In the similarity measurement method, APD was calculated as 0.79 and all the test set compounds fell within the domain of applicability as shown in Table 5. Thus, all the predictions for the test set compounds using the model may be considered reliable. In the leverages method, the warning leverage limit was observed to be 0.17, and all the test set compounds showed the leverage value below this leverage limit as shown in Table 5 which indicated that the model prediction for all the test set compounds are considered reliable. Thus, we performed both the tests (similarity measurement and leverage) and came to the conclusion that the test set compounds fell within the domain of applicability.

### Validation of the best model using external compounds reported in the literature

Nine external compounds (a–i), which were not part of the model development process, were used for external validation of the developed model. These compounds (a–i) were selected from the literature covering rimonabant (a) [56], TM38837 (b) [16], AM6545 (c) [56], cyano group-containing compounds (d–g) [57] and amide group-bearing pyrazole derivatives (h and i) [58] having the reported activity in  $\text{IC}_{50}$  values. The predictive accuracy of the best developed 3D-QSAR model (SHA) was checked by matching the predicted biological activities with the experimentally determined ones. The predicted activities of all the compounds (a–i) were found to be matching quite closely to the actual values. The residual values ranged from 0.24 to  $-0.28$  as



**Table 5** Domain of applicability of test set compounds as determined by similarity measurement and leverage method

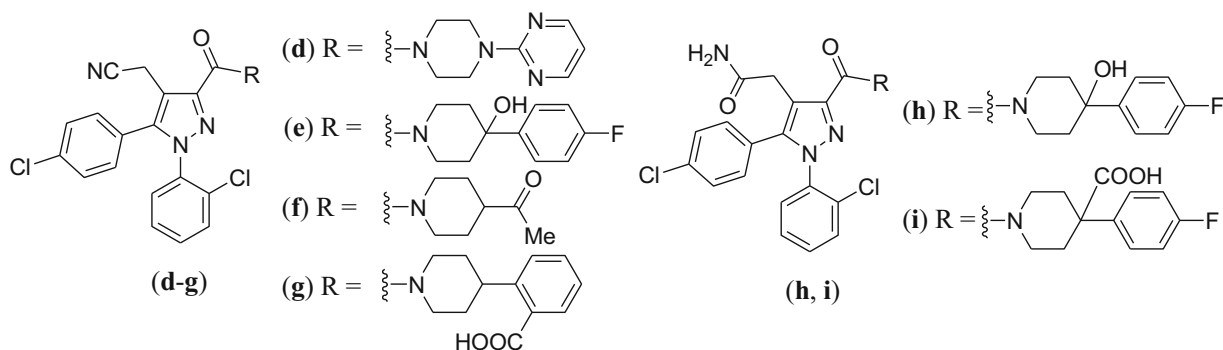
| Compounds | Similarity measurements distance (threshold APD = 0.79) | Leverage value (upper limit = 0.17) | Result   |
|-----------|---|-------------------------------------|----------|
| 1         | 0.18  | 0.03                                | Reliable |
| 5         | 0.12  | 0.04                                | Reliable |
| 9         | 0.22  | 0.05                                | Reliable |
| 12        | 0.19  | 0.02                                | Reliable |
| 19        | 0.25  | 0.04                                | Reliable |
| 21        | 0.18  | 0.04                                | Reliable |
| 23        | 0.15  | 0.05                                | Reliable |
| 37        | 0.21  | 0.05                                | Reliable |
| 38        | 0.13  | 0.04                                | Reliable |
| 39        | 0.22  | 0.05                                | Reliable |
| 42        | 0.16  | 0.05                                | Reliable |
| 49        | 0.27  | 0.04                                | Reliable |
| 50        | 0.14  | 0.02                                | Reliable |
| 54        | 0.29  | 0.13                                | Reliable |
| 58        | 0.22  | 0.08                                | Reliable |
| 61        | 0.16  | 0.05                                | Reliable |
| 62        | 0.09  | 0.05                                | Reliable |
| 65        | 0.29  | 0.08                                | Reliable |

shown in Table 6 indicating that the developed model predicted the activity quite correctly and this also proved that the correlation shown by the best developed model (SHA) was not an accidental one. Domain of applicability was also performed for these compounds as shown in Table 6. The graph of the experimental and predicted activities of the external set of compounds is shown in Fig. 6. Thus, the best developed 3D-QSAR model (SHA) could be universally utilized for further modification of the existing compounds or designing novel compounds for CB1 receptor antagonist activity.

## Graphical interpretation of contour maps

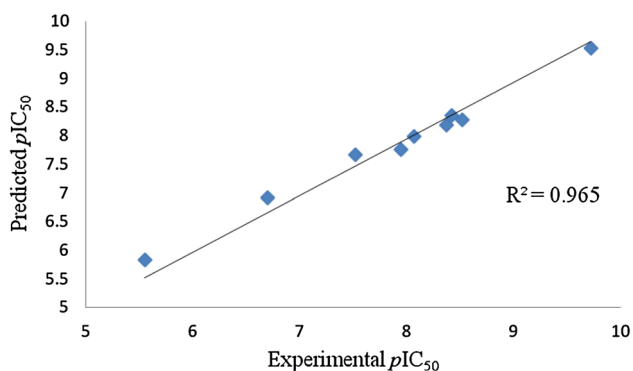
In comparison to the best CoMFA model, the best CoMSIA (SHA) model has got better predictive accuracy. The contour maps of the best developed CoMFA and CoMSIA models have been discussed. The CoMFA and CoMSIA model contour maps signify the area in space where the aligned compounds would interact favourably or unfavourably with the receptor. Visualization of contour maps is useful to gain insight into the structural requirements for CB1 receptor antagonistic activity. S and E contour maps of CoMFA model are very similar to CoMSIA contour maps. Hence, S and E contour maps of the best developed CoMFA model are discussed here.

In the CoMFA S contour maps, green-coloured contour maps (80 % contribution) represent the regions favourable for high S tolerance, while yellow-coloured contour maps (20 % contribution) represent unfavourable regions for high S tolerance. The template molecule (**20**) is shown in the contour map as shown in Fig. 7a. For the template molecule, phenyl ring at fifth position of the pyrazole is oriented towards the green region and the cyclopropane in the side chain is also surrounded by the green region. Thus, this could be the reason for good activity of the template molecule ( $IC_{50} = 0.1$  nM). Bulky substituent like oxadiazole ring in the template molecule is also present near the green region contributing positively towards the activity. *n*-Propyl chains attached to the phenyl ring at fifth position of the pyrazole ring in compound (**4**,  $IC_{50} = 1.1$  nM) and compound (**72**,  $IC_{50} = 0.5$  nM) are embedded in the green region which indicates that increasing the size of the substituents in this region may enhance the activity of the compounds. Tetrazole rings in compound (**2**,  $IC_{50} = 0.5$  nM) and compound (**3**,  $IC_{50} = 0.1$  nM) are present near the green region, oxadiazole rings in compound (**21**,  $IC_{50} = 0.8$  nM), compound (**24**,  $IC_{50} = 0.1$  nM) and compound (**25**,  $IC_{50} = 1$  nM) are enveloped in the green region. Pyridine ring of compound (**32**,  $IC_{50} = 2$  nM) is aligned towards the green region indicating that the substituents with bulkier groups in this area



**Table 6** Prediction of activity of external set of compounds (a–i) by using the best developed 3D-QSAR CoMSIA model (SHA)

| Compounds | Experimental activity ( $pIC_{50}$ ) | Predicted activity ( $pIC_{50}$ ) | Residual values | APD (0.79) | Leverage (0.17) | Result   |
|-----------|--------------------------------------|-----------------------------------|-----------------|------------|-----------------|----------|
| <b>a</b>  | 7.95                                 | 7.76                              | 0.19            | 0.64       | 0.02            | Reliable |
| <b>b</b>  | 8.07                                 | 7.99                              | 0.08            | 0.57       | 0.11            | Reliable |
| <b>c</b>  | 8.38                                 | 8.18                              | 0.20            | 0.15       | 0.06            | Reliable |
| <b>d</b>  | 8.42                                 | 8.35                              | 0.07            | 0.62       | 0.09            | Reliable |
| <b>e</b>  | 8.52                                 | 8.28                              | 0.24            | 0.10       | 0.04            | Reliable |
| <b>f</b>  | 6.70                                 | 6.91                              | −0.21           | 0.39       | 0.04            | Reliable |
| <b>g</b>  | 5.55                                 | 5.83                              | −0.28           | 0.26       | 0.06            | Reliable |
| <b>h</b>  | 9.72                                 | 9.53                              | 0.19            | 0.17       | 0.10            | Reliable |
| <b>i</b>  | 7.52                                 | 7.67                              | −0.15           | 0.27       | 0.07            | Reliable |

**Fig. 6** Graph of experimental versus predicted activities of external compounds reported in the literature

are favourable for improvement of biological activity. The cyclobutane and tetrazole rings in compound (**60**,  $IC_{50}$  = 10 nM) are present near the green region indicating moderate activity of these compounds. The phenyl ring attached to the cyclopentane of compound (**64**,  $IC_{50}$  = 14 nM) is oriented in between the green and yellow regions exhibiting moderate activity. The phenyl ring of compound (**29**,  $IC_{50}$  = 10 nM) is oriented towards the green region showing moderate activity. The presence of a thiazole ring in compound (**11**,  $IC_{50}$  = 10 nM) between the green and yellow regions may be responsible for its moderate activity. Bulky substituents of imidazo[2,1-*b*]thiazole in compound (**13**,  $IC_{50}$  = 11 nM), and *H*-imidazo[1,2-*a*]pyridine in compounds (**14**,  $IC_{50}$  = 88 nM) and compound (**15**,  $IC_{50}$  = 63 nM) are oriented towards the yellow region indicating that bulkier substituents in this region are unfavourable, hence resulting in poor activity of these compounds. The tetrazole ring of compound (**1**,  $IC_{50}$  = 145 nM) is very close to the yellow region exhibiting poor activity.

CoMFA E contour maps with template molecule (**20**) are shown in the Fig. 7b. Blue contour maps indicate the electropositive favourable (or electronegative unfavourable) regions, whereas the red contour maps indicate the elec-

tronegative favourable (or electropositive unfavourable) areas. The favourable and unfavourable regions are truncated to 85 and 15 %, respectively, to make the contour maps more clear. In the template molecule, the electronegative trifluoromethyl group and the oxygen of carbonyl group present near the red region indicate that the electronegative groups in this region are favourable for high activity. The oxygens of the ester and hydroxyl groups of compound (**71**,  $IC_{50}$  = 1 nM) and compound (**72**,  $IC_{50}$  = 0.5 nM), respectively, are present near the red region indicating good activity of these compounds. Similarly, the electronegative trifluoromethyl groups of compound (**21**,  $IC_{50}$  = 0.8 nM), compound (**24**,  $IC_{50}$  = 0.1 nM) and compound (**25**,  $IC_{50}$  = 1 nM) are present in the vicinity of the red contours favouring high activity of these compounds. The electronegative oxygen of carbonyl groups of compound (**44**,  $IC_{50}$  = 633 nM) and compound (**48**,  $IC_{50}$  = 25 nM), oxygen of hydroxyl group of compound (**48**) and oxygen of morpholine ring are present near the blue region and are unfavourable for activity, hence resulting in poor activity of the compounds. The electronegative nitrogen of tetrazole of compound (**1**,  $IC_{50}$  = 145 nM), benzimidazole ring of compound (**14**,  $IC_{50}$  = 88 nM) and piperazine rings of compound (**41**,  $IC_{50}$  = 900 nM), compound (**42**,  $IC_{50}$  = 310 nM) and compound (**43**,  $IC_{50}$  = 855 nM) are oriented towards blue region which might be responsible for their poor activity.

The CoMSIA H contour maps with template molecule (**20**) are shown in Fig. 7c. The cyan-coloured contour maps depicted the favourable regions, while the white contour maps depicted the unfavourable regions for H substituents. The contributions of favourable and unfavourable regions are truncated to 80 and 20 %, respectively. The trifluoromethyl group of the template molecule is oriented towards the cyan region which makes the compound more active. Part of the tetrazole ring of compound (**2**,  $IC_{50}$  = 0.5 nM) is present in the cyan region; trifluoromethyl group of compound (**17**,  $IC_{50}$  = 3 nM), compound (**21**,  $IC_{50}$  = 0.8 nM) and compound (**22**,  $IC_{50}$  = 0.4 nM) is present near the cyan region

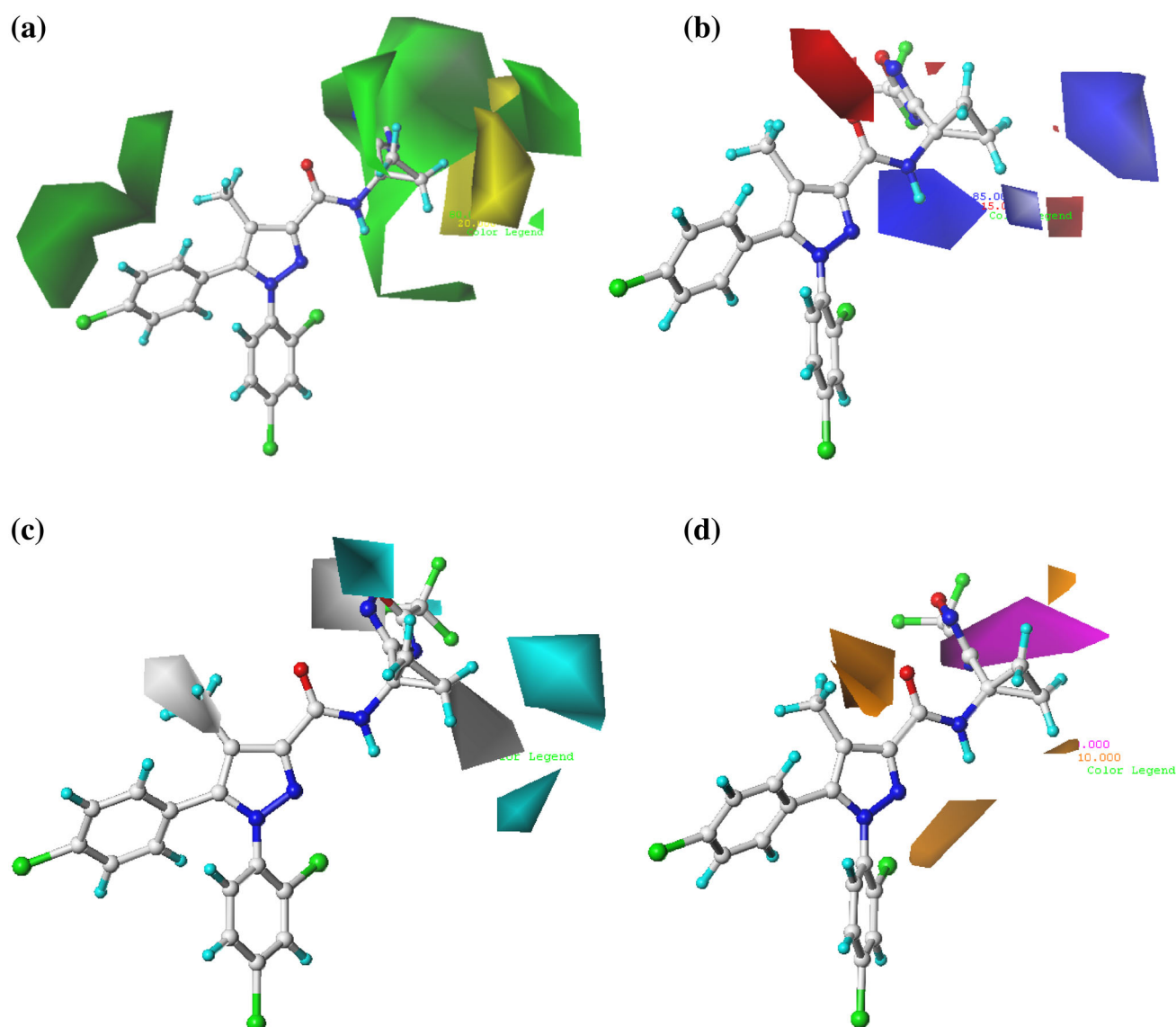


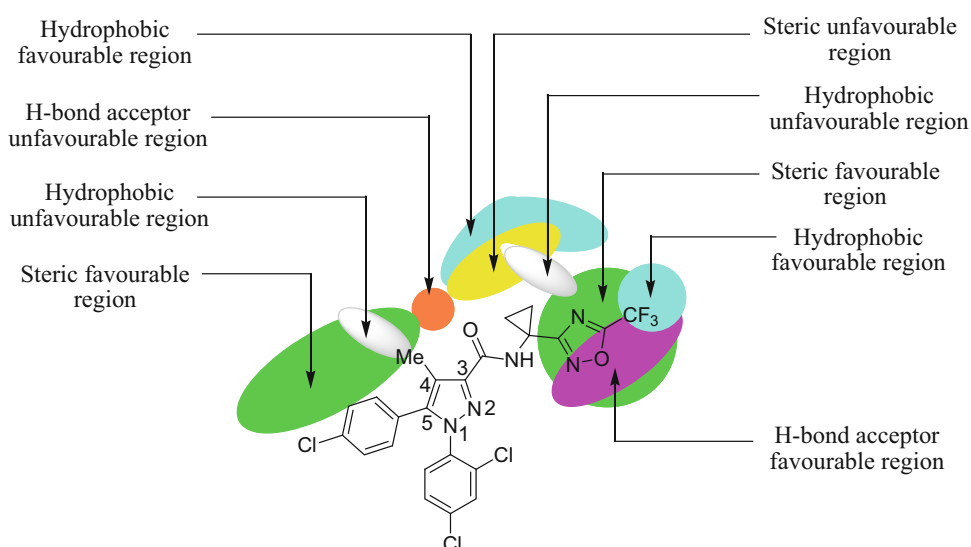
**Fig. 7** **a** CoMFA steric contour map, **b** CoMFA electrostatic contour map, **c** CoMSIA hydrophobic contour map, and **d** CoMSIA hydrogen bond acceptor contour map. (Color figure online)

indicating that substituents with H character in this region are favourable and facilitate good activity. The methyl group at position 3 of tetrazole in compound (**72**,  $IC_{50} = 0.5$  nM) is oriented near the cyan region resulting in good activity. The imidazothiazole ring of compound (**13**,  $IC_{50} = 11$  nM) is present in between cyan and white regions indicating moderate activity of this compound. The pyrazine ring of compound (**33**,  $IC_{50} = 57$  nM) is present near the white region, whereas the tetrazole ring of compound (**1**,  $IC_{50} = 145$  nM) is covered by the white region which are unfavourable for activity, thus justifying their poor activities. The tetrazole [compound (**5**,  $IC_{50} = 22$  nM)] and imidazole [compound (**36**,  $IC_{50} = 20$  nM)] rings are oriented near the white region contributing towards poor activity of these compounds.

In A CoMSIA contour maps, the magenta colour (90 % contribution) represents the region favourable for A substituents, whereas the orange-coloured contour maps (10 % contribution) represent the regions unfavourable for A groups. The template molecule (**20**) with CoMSIA A contour maps is shown in Fig. 7d. A groups like oxygen of oxadiazole ring of the template molecule embedded in the magenta region could contribute to high antagonistic activity. The oxygen of the oxadiazole of compound (**21**,  $IC_{50} = 0.8$  nM) and compound (**25**,  $IC_{50} = 1$  nM) is embedded in the magenta region justifying high activity of both the compounds. The nitrogen of tetrazole of compounds (**69**,  $IC_{50} = 8$  nM) and compound (**70**,  $IC_{50} = 3$  nM) present in between the magenta and orange regions offers moderate activity of these



**Fig. 8** Representation of contour maps of best CoMSIA model (SHA) with the template molecule (**20**). (Color figure online)

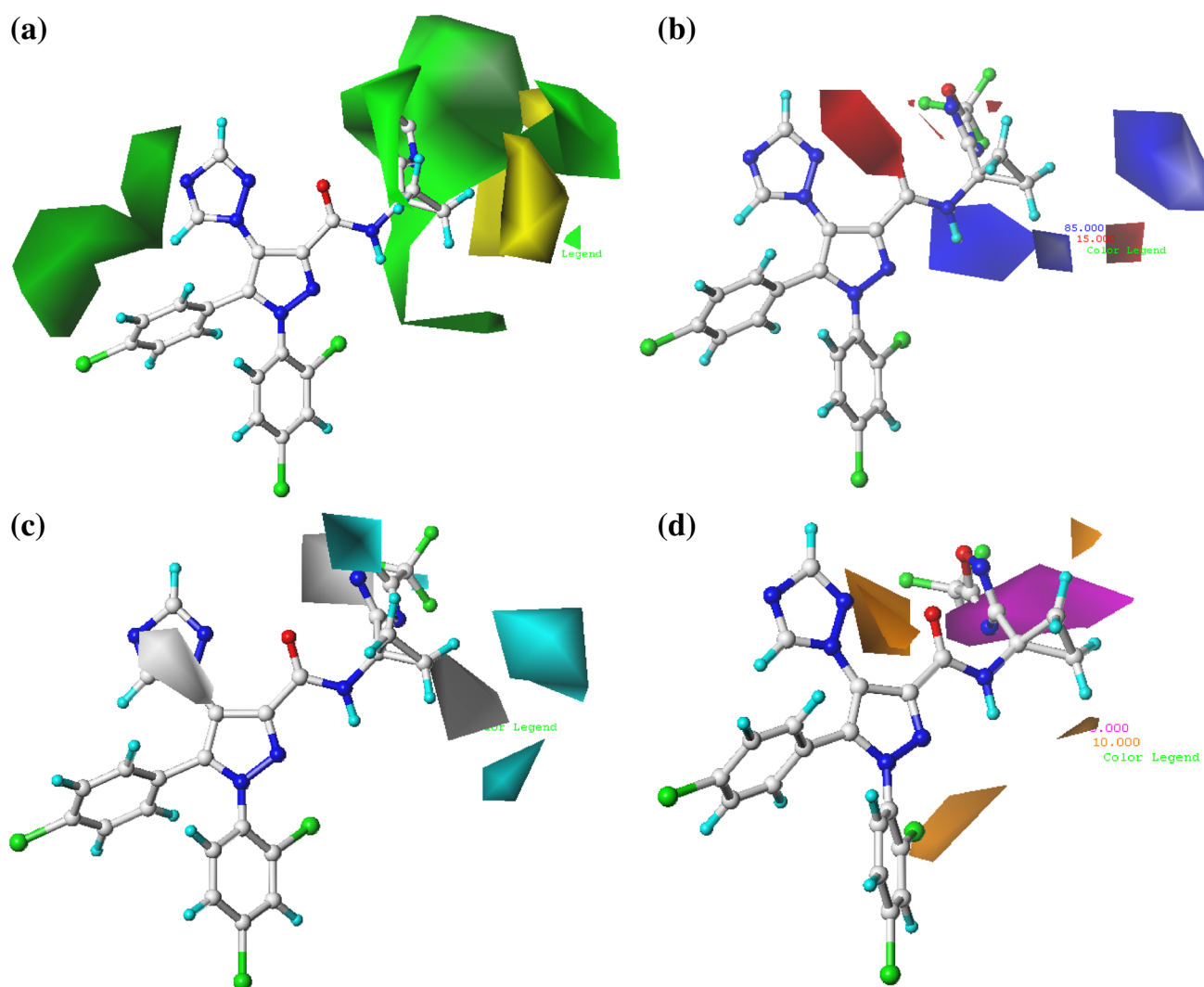


compounds. The nitrogens of tetrazole of compounds (**57**,  $IC_{50} = 100$  nM), compound (**58**,  $IC_{50} = 61$  nM), compound (**62**,  $IC_{50} = 77$  nM) and compound (**67**,  $IC_{50} = 31$  nM) are oriented towards the orange region causing poor activity of these compounds. The nitrogens of imidazole and pyrazine in compound (**35**,  $IC_{50} = 71$  nM) and compound (**33**,  $IC_{50} = 57$  nM), respectively, are oriented towards the orange region and the nitrogen of imidazopyridine of compound (**15**,  $IC_{50} = 63$  nM) is present near the orange region showing poor activity. The sulphur of the thiazole ring of compound (**8**,  $IC_{50} = 15$  nM) covered by the orange region and oxygen of the amide chain attached to the thiazole ring present near the orange region offer poor activity of the compound. Thus, the contour maps generated through the best CoMSIA model were utilized to modify the template molecule to design more potent CB1 receptor antagonists.

### Designing novel CB1 receptor antagonists using the best developed CoMSIA model (SHA)

The best developed 3D-QSAR CoMSIA (SHA) model has higher external predictive accuracy than the best CoMFA model. Hence, novel lead compounds were designed using the contour maps generated by the best CoMSIA (SHA) model with the aim to have higher CB1 receptor antagonistic activity than the template molecule (**20**). One of the main strategies adopted was to design more polar and less lipophilic derivatives so that peripherally active compounds could be designed [59]. Polarity and lipophilicity are governed by PSA and  $\log P$ , respectively. Both the properties for the compounds were calculated using Qikprop [60]. Before calculating PSA and  $\log P$  values for various compounds, the software was validated by calculating both of

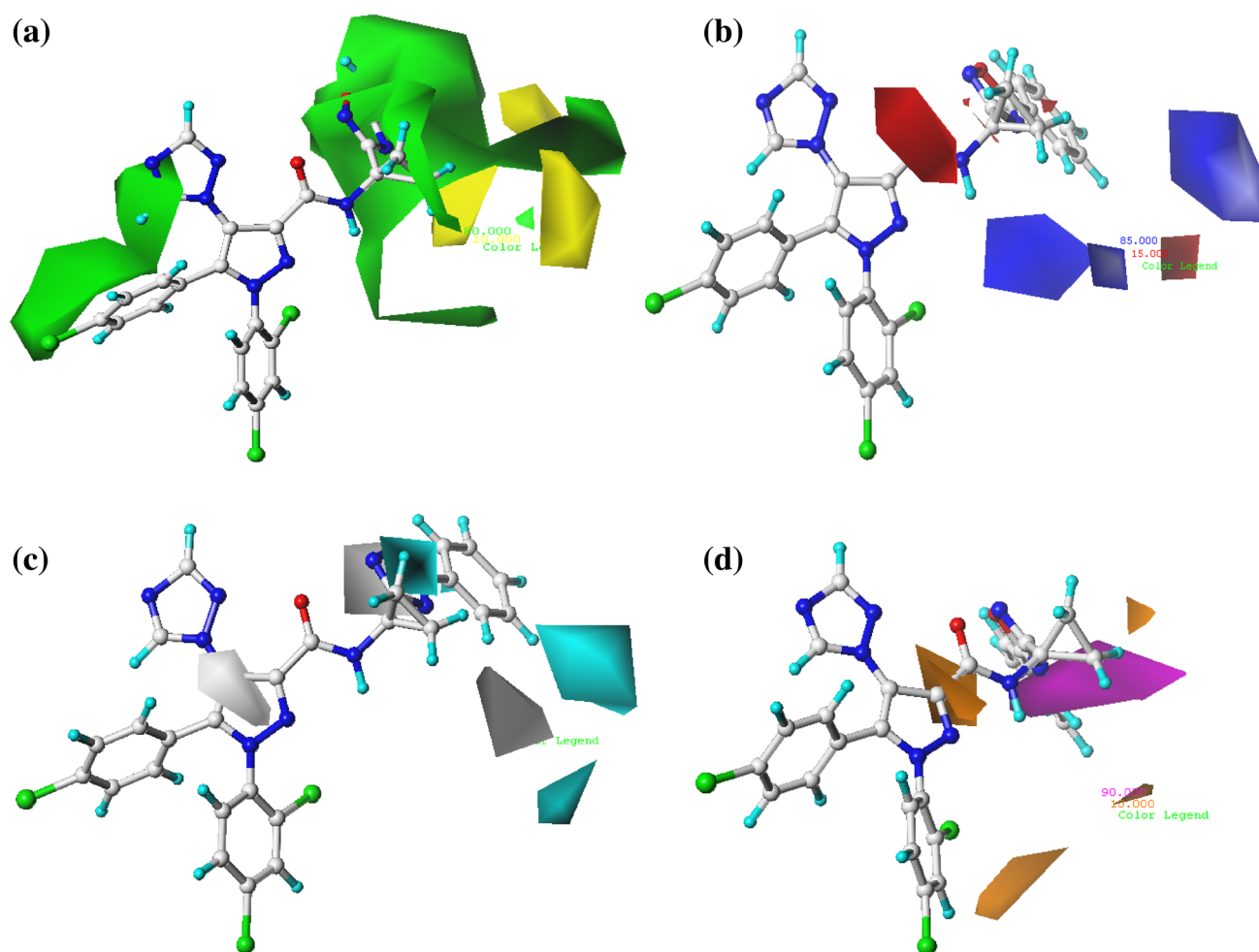
these properties for rimonabant, a known compound. The calculated values for rimonabant were found to be matching quite closely with the literature values [calculated PSA =  $53.91 \text{ \AA}^2$  (literature value =  $50.2 \text{ \AA}^2$ ); calculated  $\log P = 6.30$  (literature value =  $6.47$ )] [57]. The template molecule exhibited a PSA value of  $86.67 \text{ \AA}^2$  and a  $\log P$  of  $6.61$ . Thus, it was thought logical to modify the existing template molecule with the inputs obtained from the contour maps generated by the best CoMSIA model to design molecules with increased PSA and decreased  $\log P$  values. A lot of modifications were tried using different combinations of functional groups to enhance the biological activity of the template molecule with increased PSA and decreased  $\log P$  values. Modifications which offered better results only have been discussed here. Since the S contour maps are having green- and yellow-coloured contours for sterically favourable and unfavourable regions, respectively, efforts were made to put bulkier groups in the green region as shown in Fig. 8. Efforts were also made to put a polar and bulkier triazole group in place of the methyl group at the fourth position of the pyrazole ring in green region offering PSA and  $\log P$  values of  $106.23 \text{ \AA}^2$  and  $5.92$ , respectively, for the designed molecule. The predicted activity of this designed compound (**M1**) showed  $pIC_{50}$  value of  $9.94$  which was quite close to that of the template molecule ( $pIC_{50} = 10.00$ ). The designed compound (**M1**) fell within the domain of applicability as determined by both similarity measurement and leverage methods (Table 7). This indicated that replacement of the methyl group with triazole ring at fourth position is favourable for designing CB1 receptor antagonists. Contour maps with reference to the designed compound (**M1**) are shown in Fig. 9a–d. The triazole ring is oriented towards the green contours as shown in Fig. 9a. Further, the Cl was replaced with Br at the fourth position of the phenyl ring attached to the pyrazole ring at the fifth



**Fig. 9** Designed compound (**M1**) in **a** CoMFA steric contour map, **b** CoMFA electrostatic contour map, **c** CoMSIA hydrophobic contour map, and **d** CoMSIA hydrogen bond acceptor contour map. (Color figure online)

position and it was observed that this modification caused an increase in the activity ( $pIC_{50} = 10.04$ ) with a PSA value of  $106.23 \text{ \AA}^2$  and  $\log P$  of 5.98 for compound (**M2**). Substitution with methoxy group was also favourable resulting in increased activity ( $pIC_{50} = 10.16$ ) with increased PSA value of  $115.11 \text{ \AA}^2$  and lowered  $\log P$ , i.e., 5.50, for compound (**M3**). Green contour regions are also present on the right side covering the oxadiazole ring as shown in Fig. 8. The trifluoromethyl group was replaced with a more bulky group like phenyl which occupied the space in the green region. The biological activity of these compounds (**M4** and **M5**) also increased. Introduction of a bulkier phenyl ring in these compounds (**M4** and **M5**) increased  $\log P$ . Contour maps of the designed compound (**M5**) clearly justify the substitution of the triazole at the fourth position because the triazole ring is oriented towards green contour maps which are favourable for S groups as shown in Fig. 10a. It is very

much clear from Fig. 10d that the triazole ring is not oriented towards orange contour map (A unfavourable region). Similarly, phenyl substitution in the same region resulted in compound (**M6**) showing activity ( $pIC_{50} = 10.06$ ) with PSA  $114.31 \text{ \AA}^2$  and  $\log P$  6.15. H regions are indicated by cyan- and white-coloured contours as favourable and unfavourable regions, respectively. H favourable region is present on trifluoromethyl group attached to the oxadiazole ring as shown in Fig. 8. Substitution with H groups like iodo in this region resulted in compounds (**M7**) which increased activity ( $pIC_{50} = 10.30$ ) with a reasonable PSA value of  $109.00 \text{ \AA}^2$  and a lowered  $\log P$  value of 5.45. A contour maps are depicted with magenta and orange colours for favourable and unfavourable regions, respectively. Magenta region is covering the area of the oxadiazole ring of the template molecule (**20**) as shown in Fig. 8. So, A groups are embedded in this area. Replacement of the trifluoromethyl

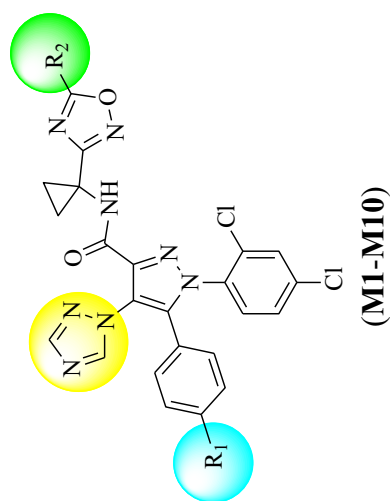


**Fig. 10** Designed compound (**M5**) in **a** CoMFA steric contour map, **b** CoMFA electrostatic contour map, **c** CoMSIA hydrophobic contour map, and **d** CoMSIA hydrogen bond acceptor contour map. (Color figure online)

with an acetyl group resulted in compound (**M8**) showing good activity  $pIC_{50} = 10.27$  with increased PSA ( $136.13 \text{ \AA}^2$ ) and lowered  $\log P$  (4.46) values. Substitution with ethyl ketone in the same region resulted in compound (**M9**) having  $pIC_{50} = 10.21$ ,  $PSA = 134.00 \text{ \AA}^2$  and  $\log P = 4.76$ . Higher activity ( $pIC_{50} = 10.61$ ) is achieved by substituting the acetyl group as A in the favourable region in compound (**M10**) showing increased PSA and lowered  $\log P$ . All the designed compounds are shown in Table 7.

Percentage oral absorption (human) and extent of CNS activities were also predicted by Qikprop. Predicted CNS activity simply indicates whether a compound is active in the CNS or inactive. The scale is  $-2$  (inactive) to  $+2$  (active). All of the designed compounds (Table 7) showed oral absorption (human) in the range of 65.97–100.00%. Rimona-bant showed CNS activity score ( $+2$ ) which indicated the penetration of the drug in the CNS, whereas the template molecule showed CNS activity score ( $+1$ ) pointing out that the tem-

plate molecule is less CNS active or more peripherally acting. The designed compounds (**M1–M7**) showed CNS activity score ( $-1$ ) meaning that these compounds are more peripherally acting than the template molecule and rimona-bant. The designed compounds (**M8–M10**) showed CNS activity score ( $-2$ ) indicating the least penetration of drug in the CNS as shown in Table 7. Hence, it can be inferred that S, H and A fields are the governing factors for designing peripherally active selective CB1 receptor antagonists. All the designed compounds have been checked for their novelty and were found to be so. The applicability domain was defined for the designed compounds (**M1–M10**) using similarity measurement and leverage methods. All designed compounds fell within the domain of applicability as shown in Table 7. The designed compound (**M10**) showed excellent in silico results and can be selected as a lead molecule for further studies.

**Table 7** Designed compounds (**M1–M10**)

| Compounds  | R <sub>1</sub> | R <sub>2</sub>  | Predicted <i>p</i> IC <sub>50</sub> | PSA           | log <i>P</i> | % Oral absorption (human) | CNS activity score | APD (0.79)  | Leverage (0.17) |
|------------|----------------|-----------------|-------------------------------------|---------------|--------------|---------------------------|--------------------|-------------|-----------------|
| <b>a</b>   |                |                 | 7.76 <sup>a</sup>                   | 53.91         | 6.30         | 100.00                    | +2                 | –           | –               |
| <b>20</b>  |                |                 | 9.75 <sup>b</sup>                   | 86.67         | 6.61         | 100.00                    | +1                 | –           | –               |
| <b>M1</b>  | Cl             | CF <sub>3</sub> | 9.94                                | 106.23        | 5.92         | 87.90                     | –1                 | 0.23        | 0.10            |
| <b>M2</b>  | Br             | CF <sub>3</sub> | 10.04                               | 106.23        | 5.98         | 88.23                     | –1                 | 0.31        | 0.16            |
| <b>M3</b>  | OMe            | CF <sub>3</sub> | 10.16                               | 115.11        | 5.50         | 72.49                     | –1                 | 0.50        | 0.02            |
| <b>M4</b>  | Cl             | Ph              | 10.06                               | 105.41        | 6.57         | 92.62                     | –1                 | 0.09        | 0.06            |
| <b>M5</b>  | Br             | Ph              | 10.66                               | 105.41        | 6.63         | 92.94                     | –1                 | 0.26        | 0.10            |
| <b>M6</b>  | OMe            | Ph              | 10.06                               | 114.31        | 6.15         | 77.19                     | –1                 | 0.27        | 0.03            |
| <b>M7</b>  | I              | I               | 10.30                               | 109.00        | 5.45         | 83.43                     | –1                 | 0.53        | 0.16            |
| <b>M8</b>  | Cl             | COMe            | 10.27                               | 136.13        | 4.46         | 65.97                     | –2                 | 0.79        | 0.07            |
| <b>M9</b>  | Cl             | COEt            | 10.21                               | 134.00        | 4.76         | 73.46                     | –2                 | 0.60        | 0.06            |
| <b>M10</b> | <b>I</b>       | <b>COMe</b>     | <b>10.61</b>                        | <b>136.13</b> | <b>4.47</b>  | <b>69.94</b>              | <b>–2</b>          | <b>0.54</b> | <b>0.13</b>     |

Bold values represent best results

<sup>a</sup> Literature value = 7.95

<sup>b</sup> Literature value = 10.00

## Conclusion

3D-QSAR CoMFA and CoMSIA models have been developed for peripherally acting 1,5-diaryl pyrazole derivatives having CB1 receptor antagonistic activity. Data-based alignment (VI) proved to be the best for CoMFA studies which was further considered for the CoMSIA studies. The best statistics was showed by CoMSIA model for a combination of S, H and A (SHA) fields which was found to be a highly predictive 3D-QSAR model. Thus, SHA are the governing field parameters for the CB1 receptor antagonistic activity of 1,5-diaryl pyrazole derivatives. The contour maps of the best CoMFA and CoMSIA models have illustrated the structural requirements for the purpose of designing of more potent and novel peripherally active CB1 receptor antagonists. Ten compounds have been designed with the help of contour maps generated through the best CoMSIA model. One designed compound (**M10**) shows very promising results having higher activity ( $pIC_{50} = 10.61$ ) than the template molecule with much higher PSA (136.13), lowered  $\log P$  (4.47), good percentage of oral absorption (human) and absence of CNS activity. The designed compound (**M10**) can be used as a lead molecule for further development of peripherally acting selective CB1 receptor antagonists.

**Acknowledgments** MKS is thankful to University Grants Commission (UGC), New Delhi for awarding Junior Research Fellowship (JRF) under the RFSMS-BSR Programme [No. F. 7-129/2007 (BSR)].

## Compliance with Ethical Standards

**Conflict of interest** The authors declare no conflict of interest in preparation of this manuscript.

## References

- <http://www.mexicobariatriccenter.com/obesity-statistics-2013-usa-world>. Accessed 13 Oct 2014
- Swinburn BA, Caterson I, Seidell JC, James WPT (2004) Diet, nutrition and the prevention of excess weight gain and obesity. *Public Health Nutr* 7:123–146. doi:10.1079/PHN2003585
- Halford JC (2001) Pharmacology of appetite suppression: implication for the treatment of obesity. *Curr Drug Targets* 2:353–370. doi:10.2174/1389450013348209
- Kirilly E, Gonda X, Bagdy G (2012) CB1 receptor antagonists: new discoveries leading to new perspectives. *Acta Physiol* 205:1–20. doi:10.1111/j.1748-1716.2011.02402.x
- <http://www.who.int/mediacentre/factsheets/fs311/en/index.html>. Accessed 13 Oct 2014
- Rodgers RJ, Tschop MH, Wilding JPH (2012) Anti-obesity drugs: past, present and future. *Dis Model Mech* 5:621–626. doi:10.1242/dmm.009621
- Powell AG, Apovian CM, Aronne LJ (2011) New drug targets for the treatment of obesity. *Clin Pharmacol Ther* 90:40–51. doi:10.1038/clpt.2011.82
- Di Marzo V, Despres JP (2009) CB1 antagonists for obesity—what lessons have we learned from rimonabant? *Nat Rev Endocrinol* 5:633–638. doi:10.1038/nrendo.2009.197
- Pertwee RG (1997) Pharmacology of cannabinoid CB1 and CB2 receptors. *Pharmacol Ther* 74:129–180. doi:10.1016/S0163-7258(97)82001-3
- Bermudez-Silva FJ, Viveros MP, McPartland JM, Rodriguez de Fonseca F (2010) The endocannabinoid system, eating behavior and energy homeostasis: the end or a new beginning? *Pharmacol Biochem Behav* 95:375–382. doi:10.1016/j.pbb.2010.03.012
- Vettor R, Pagano C (2009) The role of the endocannabinoid system in lipogenesis and fatty acid metabolism. *Best Pract Res Clin Endocrinol Metab* 23:51–63. doi:10.1016/j.beem.2008.10.002
- Yen-Ku W, Ching-Fang Y, Tai WL, Ming-Shiu H (2011) A new perspective of cannabinoid 1 receptor antagonists: approaches toward peripheral CB1R blockers without crossing the blood-brain barrier. *Curr Top Med Chem* 11:1421–1429. doi:10.2174/156802611795860997
- Kennett GA, Clifton PG (2010) New approaches to the pharmacological treatment of obesity: can they break through the efficacy barrier? *Pharmacol Biochem Behav* 97:63–83. doi:10.1016/j.pbb.2010.07.020
- Leite CE, Mocelin CA, Petersen GO, Leal MB, Thiesen FV (2009) Rimonabant: an antagonist drug of the endocannabinoid system for the treatment of obesity. *Pharmacol Rep* 61:217–224. doi:10.1016/S1734-1140(09)70025-8
- Sharma MK, Murumkar PR, Kanhed AM, Giridhar R, Yadav MR (2014) Prospective therapeutic agents for obesity: molecular modification approaches of centrally and peripherally acting selective cannabinoid 1 receptor antagonists. *Eur J Med Chem* 79:298–339. doi:10.1016/j.ejmech.2014.04.011
- Hung MS, Chang CP, Li TC, Yeh TK, Song JS, Lin Y, Wu CH, Kuo PC, Amancha PK, Wong YC, Hsiao WC, Chao YS, Shia KS (2010) Discovery of 1-(2,4-dichlorophenyl)-4-ethyl-5-(5-(2-(4-(trifluoromethyl)phenyl)ethynyl)thiophen-2-yl)-N-(piperidin-1-yl)-1H-pyrazole-3-carboxamide as a potential peripheral cannabinoid-1 receptor inverse agonist. *Chem Med Chem* 5:1439–1443. doi:10.1002/cmdc.201000246
- Clumbers LE, Fridberg M, de Kam ML, Little PB, Jensen NO, Kleinloog HD, Elling CE, van Gerven JM (2013) Peripheral selectivity of the novel cannabinoid receptor antagonist TM38837 in healthy subjects. *Br J Clin Pharmacol* 76:846–857. doi:10.1111/bcp.12141
- Quarta C, Mazza R, Obici S, Pasquali R, Pagotto U (2011) Energy balance regulation by endocannabinoids at central and peripheral levels. *Trends Mol Med* 17:518–526. doi:10.1016/j.molmed.2011.05.002
- Douguet D, Munier-Lehmann H, Labesse G, Pochet S (2005) LEA3D: a computer-aided ligand design for structure-based drug design. *J Med Chem* 48:2457–2468. doi:10.1021/jm0492296
- Wang P, Cai J, Chen J, Li L, Sun C, Xue B, Ji M (2014) 3D-QSAR and docking studies of piperidine carboxamide derivatives as ALK inhibitors. *Med Chem Res* 23:2576–2583. doi:10.1007/s00044-013-0853-4
- Murumkar PR, Giridhar R, Yadav MR (2008) 3D-quantitative structure–activity relationship studies on benzothiadiazepine hydroxamates as inhibitors of tumor necrosis factor- $\alpha$  converting enzyme. *Chem Biol Drug Des* 71:363–373. doi:10.1111/j.1747-0285.2008.00639.x
- Murumkar PR, DasGupta S, Zambre VP, Giridhar R, Yadav MR (2009) Development of predictive 3D-QSAR CoMFA and CoMSIA models for  $\beta$ -aminohydroxamic acid-derived tumor necrosis factor- $\alpha$  converting enzyme inhibitors. *Chem Biol Drug Des* 73:97–107. doi:10.1111/j.1747-0285.2008.00737.x
- Murumkar PR, Zambre VP, Yadav MR (2010) Development of predictive pharmacophore model for in silico screening, and 3D QSAR CoMFA and CoMSIA studies for lead optimization, for designing of potent tumor necrosis factor alpha converting enzyme inhibitors. *J Comput Aided Mol Des* 24:143–156. doi:10.1007/s10822-010-9322-z



24. Murumkar PR, Le L, Truong TN, Yadav MR (2011) Determination of structural requirements of influenza neuraminidase type A inhibitors and binding interaction analysis with the active site of A/H1N1 by 3D-QSAR CoMFA and CoMSIA modeling. *Med Chem Commun* 2:710–719. doi:[10.1039/c1md00050k](https://doi.org/10.1039/c1md00050k)
25. Murumkar PR, Sharma MK, Shinde AC, Bothara KG (2013) Three-dimensional quantitative structure–activity relationship CoMFA/CoMSIA on pyrrolidine-based tartrate diamides as TACE inhibitors. *Med Chem Res* 22:4192–4201. doi:[10.1007/s00044-012-0409-z](https://doi.org/10.1007/s00044-012-0409-z)
26. Murumkar PR, Sharma MK, Giridhar R, Yadav MR (2014) Virtual screening-based identification of lead molecules as selective TACE inhibitors. *Med Chem Res* 24:226–244. doi:[10.1007/s00044-014-1097-7](https://doi.org/10.1007/s00044-014-1097-7)
27. Zambre VP, Murumkar PR, Giridhar R, Yadav MR (2009) Structural investigations of acridine derivatives by CoMFA and CoMSIA reveal novel insight into their structures toward DNA G-Quadruplex mediated telomerase inhibition and Offer a highly predictive 3D-model for substituted Acridines. *J Chem Inf Model* 49:1298–1311. doi:[10.1021/ci900036w](https://doi.org/10.1021/ci900036w)
28. Zambre VP, Murumkar PR, Giridhar R, Yadav MR (2010) Development of highly predictive 3D-QSAR CoMSIA models for anthraquinone and acridone derivatives as telomerase inhibitors targeting G-quadruplex DNA telomere. *J Mol Graph Model* 29:229–239. doi:[10.1016/j.jmgm.2010.07.003](https://doi.org/10.1016/j.jmgm.2010.07.003)
29. Zambre VP, Giridhar R, Yadav MR (2013) Pharmacophore modeling and 3D-QSAR (CoMSIA) studies for structural requirements of some triazine derivatives as G-quadruplex binders for telomerase inhibition. *Med Chem Res* 22:4685–4699. doi:[10.1007/s00044-012-0447-6](https://doi.org/10.1007/s00044-012-0447-6)
30. Puntambekar DS, Giridhar R, Yadav MR (2006) 3D-QSAR CoMFA/CoMSIA studies on 5-aryl-2,2-dialkyl-4-phenyl-3(2H)-furanone derivatives, as selective COX-2 inhibitors. *Acta Pharm* 56:157–174
31. Puntambekar DS, Giridhar R, Yadav MR (2006) 3D-QSAR studies of farnesyltransferase inhibitors: a comparative molecular field analysis approach. *Bioorg Med Chem Lett* 16:1821–1827. doi:[10.1016/j.bmcl.2006.01.019](https://doi.org/10.1016/j.bmcl.2006.01.019)
32. Puntambekar DS, Giridhar R, Yadav MR (2006) Understanding the antitumor activity of novel tricyclicpiperazinyl derivatives as farnesyltransferase inhibitors using CoMFA and CoMSIA. *Eur J Med Chem* 41:1279–1292. doi:[10.1016/j.ejmech.2006.07.002](https://doi.org/10.1016/j.ejmech.2006.07.002)
33. Puntambekar DS, Giridhar R, Yadav MR (2008) Insights into the structural requirements of farnesyltransferase inhibitors as potential anti-tumor agents based on 3D-QSAR CoMFA and CoMSIA models. *Eur J Med Chem* 43:142–154. doi:[10.1016/j.ejmech.2007.02.003](https://doi.org/10.1016/j.ejmech.2007.02.003)
34. Hernandez-Vazquez E, Mendez-Lucio O, Hernandez-Luis F (2013) Activity landscape analysis, CoMFA and CoMSIA studies of pyrazole CB1 antagonists. *Med Chem Res* 22:4133–4145. doi:[10.1007/s00044-012-0418-y](https://doi.org/10.1007/s00044-012-0418-y)
35. Sasmal PK, Reddy DS, Talwar R, Venkatesham B, Balasubrahmanyam D, Kannan M, Srinivas P, Kumar KS, Devi BN, Jadhav VP, Khan SK, Mohan P, Chaudhury H, Bhuniya D, Iqbal J, Chakrabarti R (2011) Novel pyrazole-3-carboxamide derivatives as cannabinoid-1 (CB1) antagonists: journey from non-polar to polar amides. *Bioorg Med Chem Lett* 21:562–568. doi:[10.1016/j.bmcl.2010.10.055](https://doi.org/10.1016/j.bmcl.2010.10.055)
36. Sasmal PK, Talwar R, Swetha J, Balasubrahmanyam D, Venkatesham B, Rawoof KA, Devi BN, Jadhav VP, Khan SK, Mohan P, Reddy DS, Nyavanandi VK, Nanduri S, Kumar SK, Kannan M, Srinivas P, Nadipalli P, Chaudhury H, Sebastian VJ (2011) Structure–activity relationship studies of novel pyrazole and imidazole carboxamides as cannabinoid-1 (CB1) antagonists. *Bioorg Med Chem Lett* 21:4913–4918. doi:[10.1016/j.bmcl.2011.06.017](https://doi.org/10.1016/j.bmcl.2011.06.017)
37. SYBYL 7.0. Tripos, Inc., St. Louis
38. Adhikari N, Halder AK, Mondal C, Jha T (2013) Exploring structural requirements of aurone derivatives as antimalarials by validated DFT-based QSAR, HQSAR, and COMFA-COMSA approach. *Med Chem Res* 22:6029–6045. doi:[10.1007/s00044-013-0590-8](https://doi.org/10.1007/s00044-013-0590-8)
39. Cramer RD, Patterson DE, Bunce JD (1988) Comparative molecular field analysis (CoMFA). 1. Effect of shape on binding of steroids to carrier proteins. *J Am Chem Soc* 110:5959–5967. doi:[10.1021/ja00226a005](https://doi.org/10.1021/ja00226a005)
40. Zha C, Brown GB, Brouillette WJ (2014) A highly predictive 3D-QSAR model for binding to the voltage-gated sodium channel: design of potent new ligands. *Bioorg Med Chem* 22:95–104. doi:[10.1016/j.bmc.2013.11.049](https://doi.org/10.1016/j.bmc.2013.11.049)
41. Kliebe G, Abraham U, Mietzner T (1994) Molecular similarity indices in a comparative analysis (CoMSIA) of drug molecules to correlate and predict their biological activity. *J Med Chem* 37:4130–4146. doi:[10.1021/jm00050a010](https://doi.org/10.1021/jm00050a010)
42. Cramer RD, Bunce JD, Patterson DE (1988) Crossvalidation, bootstrapping, and partial least squares compared with multiple regression in conventional QSAR studies. *Quant Struct Act Relatsh* 7:18–25. doi:[10.1002/qsar.19880070105](https://doi.org/10.1002/qsar.19880070105)
43. Kamath S, Buolamwini JK (2003) Receptor-guided alignment-based comparative 3D-QSAR studies of benzylidene malonitrile typhostins as EGFR and HER-2 kinase inhibitors. *J Med Chem* 46:4657–4668. doi:[10.1021/jm030065n](https://doi.org/10.1021/jm030065n)
44. Araujo JQ, de Brito MA, Hoelz LVB, de Alencastro RB, Castro HC, Rodrigues CR, Albuquerque MG (2011) Receptor-dependent (RD) 3D-QSAR approach of a series of benzylpiperidine inhibitors of human acetylcholinesterase (HuAChE). *Eur J Med Chem* 46:39–51. doi:[10.1016/j.ejmech.2010.10.009](https://doi.org/10.1016/j.ejmech.2010.10.009)
45. Dunn WJ, Wold S, Edlund V, Helberg S (1984) Multivariate structure–activity relationship between data from a battery of biological tests and an ensemble of structure descriptors: the PLS method. *Quant Struct Act Relatsh* 3:131–137. doi:[10.1002/qsar.19840030402](https://doi.org/10.1002/qsar.19840030402)
46. Hansch C, Verma RP (2009) Overcoming tumor drug resistance with C<sub>2</sub>-modified 10-deacetyl-7-propionyl cephalomannines: a QSAR study. *Mol Pharm* 6:849–860. doi:[10.1021/mp800138w](https://doi.org/10.1021/mp800138w)
47. Verma RP, Hansch C (2008) Combating the threat of anthrax: a quantitative structure–activity relationship approach. *Mol Pharm* 5:745–759. doi:[10.1021/mp8000149](https://doi.org/10.1021/mp8000149)
48. Kristama R, Parmara V, Viswanadhana VN (2013) 3D-QSAR analysis of TRPV1 inhibitors reveals a pharmacophore applicable to diverse scaffolds and clinical candidates. *J Mol Graph Model* 45:157–172. doi:[10.1016/j.jmgm.2013.08.014](https://doi.org/10.1016/j.jmgm.2013.08.014)
49. Liu Y, Lu X, Xue T, Hu S, Zhang H (2014) Receptor and ligand-based 3D-QSAR study on a series of pyrazines/pyrrolidylquinazolines as inhibitors of PDE10A enzyme. *Med Chem Res* 23:775–789. doi:[10.1007/s00044-013-0619-z](https://doi.org/10.1007/s00044-013-0619-z)
50. Roy PP, Paul S, Mitra I, Roy K (2009) On two novel parameters for validation of predictive QSAR models. *Molecules* 14:1660–1701. doi:[10.3390/molecules14051660](https://doi.org/10.3390/molecules14051660)
51. Roy PP, Roy K (2008) On some aspects of variable selection for partial least squares regression models. *QSAR Comb Sci* 27:302–313. doi:[10.1002/qsar.200710043](https://doi.org/10.1002/qsar.200710043)
52. Golbraikh A, Tropsha A (2002) Beware of q<sup>2</sup>!. *J Mol Graph Model* 20:269–276. doi:[10.1016/S1093-3263\(01\)00123-1](https://doi.org/10.1016/S1093-3263(01)00123-1)
53. Melagraki G, Afantitis A (2013) Enalos KNIME nodes: exploring corrosion inhibition of steel in acidic medium. *Chemom Intell Lab Syst* 123:9–14. doi:[10.1016/j.chemolab.2013.02.003](https://doi.org/10.1016/j.chemolab.2013.02.003)
54. Zhang S, Golbraikh A, Oloff S, Kohn H, Tropsha A (2006) A novel automated lazy learning QSAR (ALL-QSAR) approach: method development, applications, and virtual screening of chemical databases using validated ALL-QSAR models. *J Chem Inf Model* 46:1984–1995. doi:[10.1021/ci060132x](https://doi.org/10.1021/ci060132x)

55. Melagraki G, Afantitis A (2014) Enalos InSilicoNano platform: an online decision support tool for the design and virtual screening of nanoparticles. *RSC Adv* 4:50713–50725. doi:[10.1039/C4RA07756C](https://doi.org/10.1039/C4RA07756C)
56. Dossou KS, Devkota KP, Kavanagh PV, Beutler JA, Egan JM, Moaddel R (2013) Development and preliminary validation of a plate-based CB1/CB2 receptor functional assay. *Anal Biochem* 437:138–143. doi:[10.1016/j.ab.2013.02.025](https://doi.org/10.1016/j.ab.2013.02.025)
57. Cooper M, Receveur JM, Bjurling E, Norregaard PK, Nielsen PA, Skold N, Hogberg T (2010) Exploring SAR features in diverse library of 4-cyanomethyl-pyrazole-3-carboxamides suitable for further elaborations as CB1 antagonists. *Bioorg Med Chem Lett* 20:26–30. doi:[10.1016/j.bmcl.2009.11.047](https://doi.org/10.1016/j.bmcl.2009.11.047)
58. Receveur J-M, Murray A, Linget J-M et al (2010) Conversion of 4-cyanomethyl-pyrazole-3-carboxamides into CB1 antagonists with lowered propensity to pass the blood–brain-barrier. *Bioorg Med Chem Lett* 20:453–457. doi:[10.1016/j.bmcl.2009.12.003](https://doi.org/10.1016/j.bmcl.2009.12.003)
59. Sharma MK, Murumkar PR, Barmade MA, Giridhar R, Yadav MR (2015) A comprehensive patents review on cannabinoid 1 receptor antagonists as antiobesity agents. *Expert Opin Ther Pat*. doi:[10.1517/13543776.2105.1064898](https://doi.org/10.1517/13543776.2105.1064898)
60. Qikprop version 3.2. Schrödinger, LLC, New york (2009)